Economic Geology, v. 117, no. 6, pp. 1299–1326

Lithostratigraphy, Lithogeochemistry, and Tectono-Magmatic Framework of the ABM Replacement-Style Volcanogenic Massive Sulfide (VMS) Deposit, Finlayson Lake District, Yukon, Canada

Nikola Denisová† and Stephen J. Piercey

Department of Earth Sciences, Memorial University of Newfoundland, St. John's, Newfoundland A1B 3X5, Canada

Abstract

The Upper Devonian ABM deposit is a bimodal-felsic, replacement-style volcanogenic massive sulfide (VMS) deposit within the Finlayson Lake district in Yukon, Canada. The deposit is hosted by predominantly felsic volcanic rocks of the upper Kudz Ze Kayah formation that were deposited in an active back-arc basin in three sequences consisting of interbedded felsic volcaniclastic rocks and argillites, and felsic lava flows and domes, and felsic and mafic sills. The felsic rocks fall into two groups, Felsic A and Felsic B (FA and FB), based on immobile elements and their ratios. Relative to the FB group, the FA group has high Zr concentrations (>550 ppm) and generally higher contents of high field strength elements. The FA/FB chemostratigraphy roughly coincides with the lithostratigraphic sequences. Sequence 2 hosting the mineralization consists of FB felsic rocks; the hanging-wall Sequence 3 and footwall Sequence 1 felsic rocks have FA signatures. An argillite lens, recording a period of volcanic quiescence, occurs at the upper contact of Sequence 2.

From reconstruction of the basin architecture, two sets of synvolcanic faults are inferred. The synvolcanic faults were interpreted based on thickness changes of volcanosedimentary units and the distribution of coherent rocks. During breaks in volcanism, synvolcanic faults acted as conduits for upwelling hydrothermal fluids, which were diverted laterally into unconsolidated volcaniclastic rocks and formed the replacement-style VMS mineralization. Although the mineralized lenses are hosted by FB felsic rocks, their replacement-style nature implies that the mineralizing processes occurred during the break in volcanism and were genetically associated with the overlying FA felsic volcanic rocks.

Introduction

Volcanogenic massive sulfide (VMS) deposits form in extensional environments at or near the sea floor by the mixing of cold seawater with hot hydrothermal fluids (Franklin et al., 1981, 2005; Tornos et al., 2015). The efficiency of the mineralizing processes is highest where the mixing of metal-rich hydrothermal fluids with seawater occurs in the subsurface, which results in relatively larger tonnages and higher grades of replacement-style VMS deposits when compared to mound-style (exhalative) deposits that formed on the sea floor (Allen et al., 2002; Doyle and Allen, 2003; Piercey, 2015). Despite the challenge of replacement texture identification in deformed and metamorphosed rocks, many deposits have lower strain zones where these features can be recognized (Doyle and Allen, 2003; Piercey, 2015; Lafrance et al., 2020), and when integrated with the stratigraphic reconstruction, architecture, and tectonic framework of basins (Allen et al., 1996a, b; Winter et al., 2004; Thurston et al., 2008; Belford et al., 2015; DeWolfe et al., 2018; Friesen et al., 2020) and lithogeochemistry of the host rocks (Barrett and MacLean, 1994; Barrett et al., 2001), an enhanced understanding of both ancient and recent VMS deposits and their emplacement mechanisms can be achieved. Variations to this approach utilizing detailed stratigraphic facies analysis and lithostratigraphic reconstruction have been applied on numerous replacement-style VMS deposits of various ages globally, including the Abitibi district (Ansil deposit; Galley et al., 1995), the Mount Read Volcanics in Tasmania (South Hercules deposit; Zaw and Large, 1992), the Mount Windsor subprovince in Australia (Highway Reward deposit; Doyle and Huston, 1999), the Appalachians in Canada (Boundary deposit; Piercey et al., 2014), the Skellefte district in Sweden (Allen et al., 1996b), and the Iberian Pyrite Belt in Spain and Portugal (Tornos, 2006). Further research focusing on reconstructing the basin architecture of the deposit-hosting extensional basins will help to illuminate the more cryptic aspects of replacement-style mineralization, such as the character of hydrothermal up-flow zones, the role of synvolcanic faults, and the timing of VMS mineralization in relation to volcanism and processes in underlying magma chambers.

The Finlayson Lake district, Yukon, Canada, consists of arc and back-arc rocks of the Yukon-Tanana and Slide Mountain terranes and hosts various styles of VMS deposits with >40 Mt of reported polymetallic VMS mineralization. The ABM deposit is a bimodal-felsic, replacement-style VMS deposit that contains a mineral resource of 19.1 Mt @ 6.6 wt % Zn, 0.9 wt % Cu, 2.0 wt % Pb, 1.4 g/t Au, and 156 g/t Ag (van Olden et al., 2020). The ABM deposit is one of five polymetallic VMS deposits discovered in the district in the 1990s that initiated a number of regional-scale (Murphy, 1998; Piercey, 2001; Piercey et al., 2001, 2003; Murphy et al., 2006; Manor and Piercey, 2019) and deposit-scale studies (Boulton, 2002; Sebert et al., 2004; Peter et al., 2007; Layton-Matthews et al., 2013; McDonald et al., 2018), with particular attention paid to the Zn-enriched Wolverine deposit (Bradshaw et al., 2008; Piercey et al., 2008, 2016; Piercey and Kamber, 2019). In 2015, an extensive drilling campaign (BMC Minerals Ltd.) further delineated the ABM deposit and led to the discovery of the

†Corresponding author: e-mail, ndenisova@mun.ca

 Submitted: June 28, 2021 / Accepted: December 14, 2021

Krakatoa mineralized zone in the immediate vicinity of the ABM deposit (van Olden et al., 2020). This discovery renewed interest in the mineralization potential of the host rocks in the Finlayson Lake district, as much of the area remains underexplored. The new discovery and the recently reinterpreted replacement-style nature of the massive sulfide mineralization (van Olden et al., 2020; Manor et al., in press) call for further study and reevaluation of the lithostratigraphic and tectonic framework of the ABM deposit. The relatively low degree of metamorphism and deformation together with abundant available drill core from the deposit and its vicinity make the ABM deposit an ideal site to study an Upper Devonian back-arc basin environment that hosts replacement-style VMS mineralization. This study uses detailed core logging, lithofacies analysis, and lithogeochemistry to 1) create a reconstruction of the ABM deposit with respect to its lithostratigraphy and tectonic framework, 2) determine what specific characteristics of the reconstructed environment are linked to the replacement-style VMS mineralization at the ABM deposit, and 3) compare our results with previous larger-scale petrogenetic and metallogenic studies in the Finlayson Lake district to test and evaluate them. The collected data and derived interpretations are presented in this paper in the form of long sections and cross sections through the deposit. Our results highlight the Late Devonian back-arc basin architecture during which the bimodal, but mostly felsic, volcanism and associated VMS mineralization occurred. The diagnostic features of VMS mineralization in the ABM deposit, including the lithostratigraphy, lithogeochemistry, and structure, are defined in this study and have potential to be utilized in further exploration in the Finlayson Lake district, the northern Cordillera, and analogous ancient environments worldwide

Regional Geology

The Finlayson Lake district in southeastern Yukon is a dismembered block of the Yukon-Tanana and Slide Mountain terranes that developed along the western margin of Laurentia throughout the Mid-Paleozoic to the Permo-Triassic (Fig. 1; Colpron et al., 2006; Nelson et al., 2006; Piercey et al., 2006). The Yukon-Tanana terrane is an allochthonous peri-Laurentian package that consists of distinct arc–back-arc assemblages that underlie parts of Yukon, Alaska, and northern British Columbia (Nelson et al., 2006). It comprises a polydeformed and metamorphosed pre-Late Devonian continental margin assemblage (Snowcap assemblage; Piercey and Colpron, 2009) that is overlain by three unconformity-bound Late Devonian to Middle to Late Permian continental arc, back-arc, and ocean basin-related volcano-sedimentary sequences that underwent variable degrees of metamorphism and deformation (Mortensen and Jilson, 1985; Mortensen, 1992; Colpron et al., 2006; Murphy et al., 2006). The pre-Late Devonian basement of the Yukon-Tanana terrane is not exposed in the Finlayson Lake district, but is characterized as Laurentian-derived, pericontinental crustal material (Piercey et al., 2001, 2003, 2017; Piercey and Colpron, 2009). In the Eocene, the Finlayson Lake district was displaced from its original location approximately 430 km along the dextral strike-slip Tintina fault (Gabrielse et al., 2006).

The Finlayson Lake district is composed of Late Devonian to Permian metasedimentary, metavolcanic, and plutonic rocks that have undergone variable degrees of deformation (Murphy et al., 2006). The core of the Finlayson Lake district reached amphibolite facies metamorphic grade, which transitions to lower greenschist facies further from the center of the district (Murphy et al., 2006). The rocks of the Yukon-Tanana terrane in the Finlayson Lake district occur in three structurally bounded stratigraphic sequences: the Big Campbell, Money Creek, and Cleaver Lake thrust sheets (Fig. 2). The largest of these blocks by volume is the structurally deepest Big Campbell thrust sheet, which consists of Upper Devonian metaclastic rocks of the North River formation, the Upper Devonian Grass Lakes group, and the Lower Mississippian Wolverine Lake group (Fig. 2; Murphy et al., 2006). The Grass Lakes group comprises three rock units: the Fire Lake, Kudz Ze Kayah, and Wind Lake formations (Fig. 2). The Fire Lake formation comprises mafic metavolcanic and lesser amounts of mafic and ultramafic meta-subvolcanic rocks (Piercey et al., 2002a; Murphy et al., 2006), and hosts the Kona Cu-Co VMS deposit (Sebert et al., 2004; Peter et al., 2007) containing a geologic resource of 10.5 Mt @ 1.6 wt % Cu, 0.63 g/t Au, and 4 g/t Ag (BMC Minerals). The Kudz Ze Kayah formation is interpreted to be stratigraphically above the Fire Lake formation and is characterized by dominantly felsic volcanic and sedimentary rocks with back-arc geochemical affinities (Piercey et al., 2001; Murphy et al., 2006). The Wind Lake formation sits conformably on top of the Kudz Ze Kayah formation and consists of interlayered carbonaceous sedimentary rocks and alkalic mafic volcanic rocks with minor quartzite (Piercey et al., 2002b). All rocks in the Grass Lakes group are intruded by the Grass Lakes plutonic suite at ca. 361 Ma (Piercey et al., 2001, 2003; Manor et al., 2022). The Wolverine Lake group unconformably overlies the Grass Lakes group and contains basal conglomerates, sandstones, felsic volcanic rocks, carbonaceous phyllite/shale, ironstones, and basaltic rocks (Murphy and Piercey, 1999; Bradshaw et al., 2001). The Wolverine felsic-siliciclastic type VMS deposit lies on the contact between carbonaceous phyllite and felsic volcanic rocks and contains a geologic resource of 6.2 Mt @ 12.9 wt % Zn, 1.5 wt % Pb, 1.4 wt % Cu, 1.81 g/t Au, and 359 g/t Ag (Bradshaw et al., 2008). Structurally above the Big Campbell thrust sheet sits the Money Creek thrust sheet, which is made up of rocks of the same age but formed primarily in an arc environment (Murphy et al., 2006). The Cleaver Lake thrust sheet comprises Late Devonian through Early Mississippian and Early Permian rocks formed in an arc environment and is the uppermost structural panel (Murphy et al., 2006).

VMS mineralization in the Kudz Ze Kayah formation

The ABM deposit and the GP4F VMS deposit are located about 25 km south of Finlayson Lake and the Robert Camp-

Fig. 1. Regional geologic setting of the Finlayson Lake district, Yukon-Tanana, and Slide Mountain terranes (modified after Murphy et al., 2006). Numbers mark the positions of known VMS deposits in the region. Abbreviations: BCT = Big Campbell thrust; CLT = Cleaver Lake thrust; JCF = Jules Creek fault; MCT = Money Creek thrust; NRF = North River thrust.

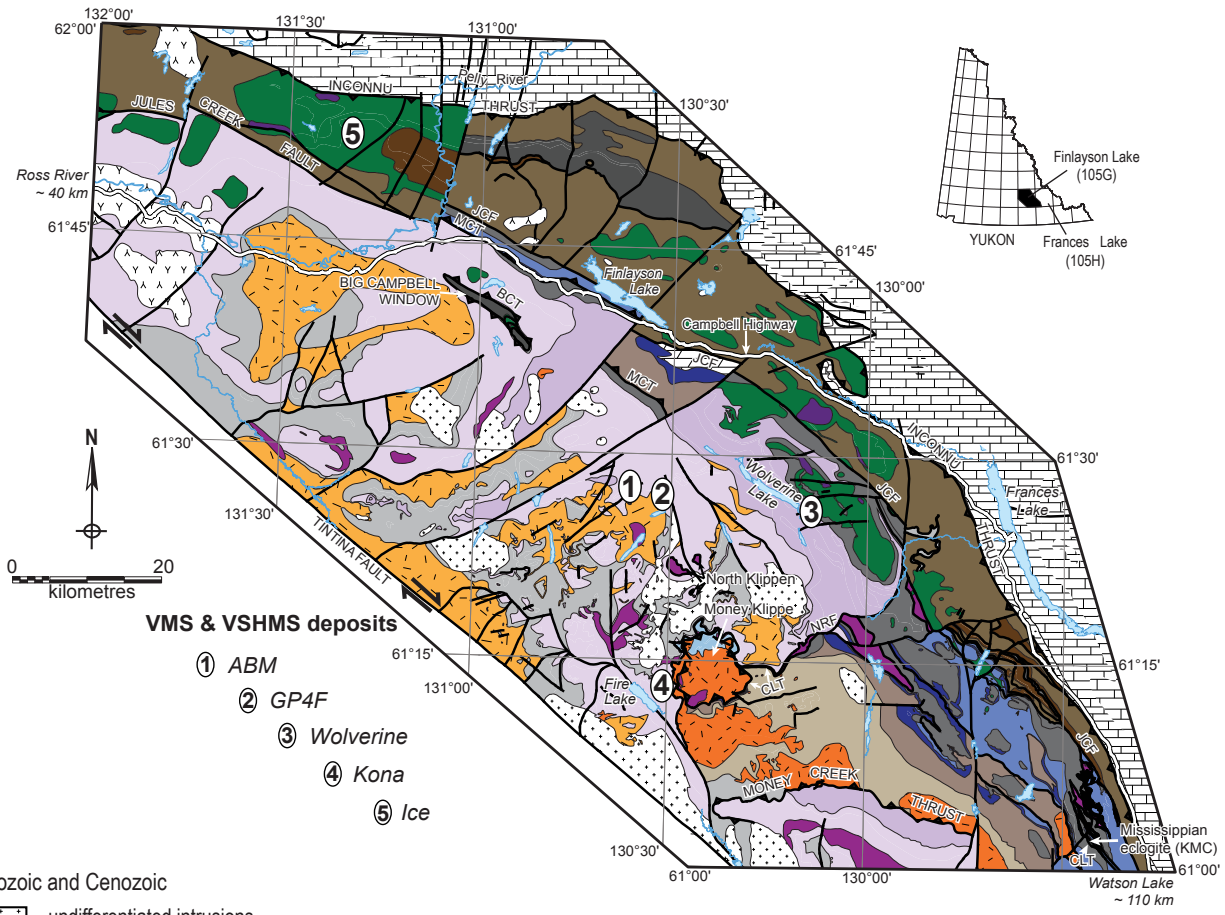

Mesozoic and Cenozoic

undifferentiated intrusions

undifferentiated volcanic rocks

North American Continental Margin

Triassic

dark shale, siltstone and limestone

Paleozoic

undifferentiated formations of Selwyn Basin, Cassiar/McEvoy Platform, Earn Group and Mt. Christie Formation

Post - YTT / SMT Amalgamation

Triassic

grey shale, siltstone and limestone

Permian - Triassic

SIMPSON LAKE GROUP

polymictic conglomerate, sandstone, siltstone, mafic and felsic volcanic rocks, limestone

Slide Mountain terrane

INTRUSIVE ROCKS

Early Permian

ultramafic and mafic intrusions

LAYERED ROCKS

Lower to Middle Permian

Gatehouse formation

limestone and quartzite

Slide Mountain terrane

Lower Permian

Campbell Range formation

basalt and varicoloured chert

Carboniferous to Permian?

FORTIN CREEK GROUP

dark phyllite and chert, varicoloured chert, chert-pebble conglomerate, sandstone, limestone, felsic and mafic metavolcanic rocks

Yukon-Tanana terrane

INTRUSIVE ROCKS

Early Mississippian

SIMPSON RANGE PLUTONIC SUITE

granite, quartz monzonite, granodiorite

Late Devonian to Early Mississippian

GRASS LAKES PLUTONIC SUITE

granite, quartz monzonite augen granite

ultramafic and mafic rocks, Big Campbell and Cleaver Lake thrust sheets

LAYERED ROCKS

Lower Permian

Money Creek formation

dark phyllite and sandstone, chert, chert-pebble conglomerate, diamictite

Mid-Pennsylvanian to Lower Permian

Finlayson Creek limestone

massive bioclastic limestone

Yukon-Tanana terrane

Upper Mississippian to mid-Pennsylvanian

undifferentiated White Lake and King Arctic formations

green and pink chert, limestone, sandstone, conglomerate, mafic metavolcanic rocks

Upper Mississippian

Whitefish limestone

massive bioclastic limestone

Lower Mississippian

Tuchitua River formation

intermediate, felsic and mafic volcanic rocks, sandstone, chert, limestone

WOLVERINE LAKE GROUP

undifferentiated mafic and felsic volcanic rocks and dark clastic rocks

Upper Devonian to Lower Mississippian

Cleaver Lake formation

calc-alkaline basalt, rhyolite, chert and volcanic-derived sandstone

Waters Creek formation

felsic to intermediate metavolcanic rocks and carbonaceous phyllite

GRASS LAKES GROUP

undifferentiated mafic and felsic volcanic rocks and dark clastic rocks of the Fire Lake, Kudz Ze Kayah and Wind Lake formations

Pre-Upper Devonian

North River formation

quartzose metaclastic rocks, marble and non-carbonaceous pelitic schist

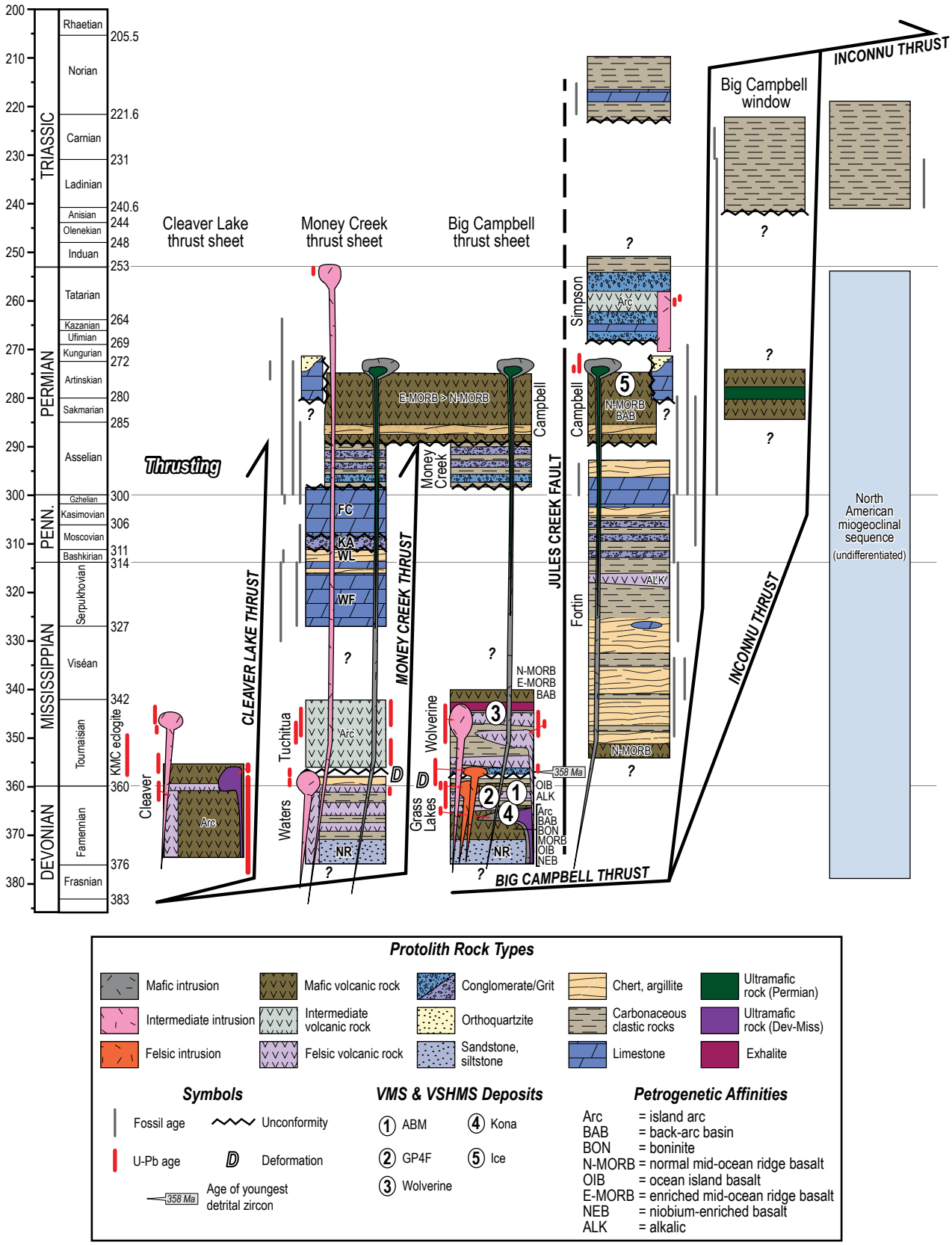

Fig. 2. Composite chronostratigraphic column for the Finlayson Lake district showing stratigraphic and structural relationships. Locations of volcanogenic massive sulfide (VMS) deposits, petrogenetic affinities of volcanic rocks and U-Pb and fossil ages displayed on diagram (modified after Murphy et al., 2006; Piercey et al., 2016; Manor and Piercey, 2018). VSHMS = volcanic sediment-hosted massive sulfide.

bell Highway (Fig. 1). The deposits were discovered in the early 1990s by Cominco, following surficial geochemical surveys, and subsequently drilled between 1994 and 1998 (Peter et al., 2007). The GP4F deposit is located roughly 5 km southeast of the ABM deposit (Fig. 1) and sits 500 to 600 m stratigraphically below the ABM deposit (Peter et al., 2007; Manor et al., in press), which itself sits roughly 150 to 250 m below the contact between the Kudz Ze Kayah and Wind Lake formations. Subseafloor replacement is interpreted to be the primary mineralization style in both deposits (Peter et al., 2007; van Olden et al., 2020; Manor et al., in press), with the most common ore minerals being pyrite, pyrrhotite, sphalerite, chalcopyrite, and galena, and the most common gangue minerals being barite, carbonate, chlorite, quartz, white mica, and Fe carbonate. The GP4F deposit has a geologic resource of 1.5 Mt at 6.4% Zn, 3.1% Pb, 0.1% Cu, 2.0 g/t Au, and 81.7 g/t Ag (MacRobbie and Holroyd, unpub. data) and was described by Boulton (2002). Previous studies of the ABM deposit defined the deposit as an isoclinally folded massive sulfide lens (Peter et al., 2007; Layton-Matthews et al., 2008, 2013); however, more recent (2015–2018) extensive drilling in the deposit area shows replacement-style textures within the orebodies and does not show any evidence of significant folding. A chronostratigraphic study by Manor et al. (in press) dated the rocks hosting the GP4F deposit formed at ca. 363.254 ± 0.098 Ma, and that the ABM deposit is hosted by rocks formed at ca. 362.82 ± 0.12 Ma. Manor et al. (in press) have also suggested that the volcanic activity responsible for the deposition of the Kudz Ze Kayah formation lasted approximately 0.65 to 1.0 m.y., which indicates rapid deposition and emplacement of volcano-sedimentary rocks played an important role in the formation of both VMS deposits.

Geology, Lithofacies, Mineralization, and Alteration of the ABM Deposit

Observations and sampling methodology

A total of 51 drill holes and ~10 km of core were logged at 1:400 scale. Graphic logging for each unit recorded lithology, primary textures, grain size, mineralogy, and alteration type and intensity based on mineral occurrence (quartz, white mica, chlorite, biotite, carbonates, and sulfides). Hydrothermal alteration associated with VMS mineralization and greenschist facies metamorphism affected the Kudz Ze Kayah formation in the area of the deposit, but distinguishable primary textures and relationships between units are preserved in significant sections of the stratigraphy (Piercey et al., 2001; this study). All rock names are presented without metamorphic prefixes, and primary volcanic and sedimentary terminology is used to highlight the remnant primary features observed in the rocks. Volcaniclastic rocks are classified using the nomenclatures outlined in White and Houghton (2006) and Fisher (1966). These classification schemes are based on clast size and abundance and are used with no genetic implications. Sampling aimed to acquire a comprehensive collection of the most common lithofacies and alteration styles distributed in the ABM deposit. Overall, 478 samples were collected. Petrographic studies of 82 samples representing the major lithostratigraphic facies are incorporated in the descriptions below. Presented stratigraphic sections and 3-D digital models of lithostratigraphic units, lenses of mineralization, and faults are based primarily on the detailed drill logs of this study. To further constrain the modeled units, core photographs, logs and assays provided by BMC Minerals Ltd. were utilized. Company data sets were only used as supportive, not principal, sources of data, apart from the Ba values. All models and interpretations carry a higher degree of uncertainty due to the limited extent of the drilling below the mineralized horizon. Digital models were created using Leapfrog Geo 5.0 software developed by Seequent.

Geology of the upper Kudz Ze Kayah formation

Rocks that host the ABM deposit occupy the top ~350 m of the >500-m-thick Kudz Ze Kayah formation. The stratigraphy dips between 20° and 30° to the north-northeast and is relatively intact, as field observations and stratigraphic reconstructions do not indicate any fault repetition or major folding. The East fault is a regional-scale fault and divides the deposit area into two zones: the ABM zone and the Krakatoa zone (Fig. 3). The ABM deposit occurs 200 ± 50 m below the transitional contact between the Kudz Ze Kayah and Wind Lake formations. The Wind Lake formation consists of interbedded mafic tuff and argillite near and at the contact with the Kudz Ze Kayah formation. Primary bedding (S_0) is recognized in argillite and mafic tuff of the Wind Lake formation, with S_1 subparallel to S_0; this is observed in argillite and strongly altered units with abundant mica and chlorite (van Olden et al., 2020). Minor S_2 folds and crenulation occur within argillites and rocks with a higher degree of alteration in both formations, but these are not indicative of any large-scale patterns on a deposit scale (van Olden et al., 2020). Lithostratigraphic units are commonly continuous over hundreds of meters, but several of them, such as the mafic sills, argillite lenses and some felsic sills can be traced up to 500 to 1,000 m throughout the ABM or Krakatoa zones. The upper portion of the Kudz Ze Kayah formation can be informally divided into three sequences based on the graphic drill logs (Fig. 4), from stratigraphically oldest to youngest: Sequence 1, Sequence 2, and Sequence 3. The Krakatoa zone generally corresponds in stratigraphy to the ABM zone but contains more voluminous volcanic and subvolcanic rocks.

Each sequence consists of interbedded felsic volcaniclastic rocks and minor sedimentary rocks, and domes and flows, that were intruded by felsic sills and mafic sills and dikes. The lithofacies are described in detail below. Sequence 1 is the lowermost stratigraphic sequence and consists of interbedded felsic tuff, lapilli tuff, felsic subvolcanic rocks, and rare argillite lenses. Its lower contact is unknown due to minimal drilling below the mineralized horizon but extends at least a minimum of 100 m below the contact between Sequence 1 and Sequence 2. Sequence 2 hosts the mineralization and consists of interbedded felsic tuff and lapilli tuff and minor argillite lenses and contains felsic lava flows, two mafic sills, and abundant felsic sills. In the ABM zone, Sequence 2 varies in thickness between 45 and 120 m (average ~100 m), and generally thins down-dip towards the north-northeast. Its lower boundary is defined by the lower contact of the deepest mafic sill; the upper boundary is located at the laterally most extensive argillite lens. Sequence 2 in the Krakatoa zone consists pre-

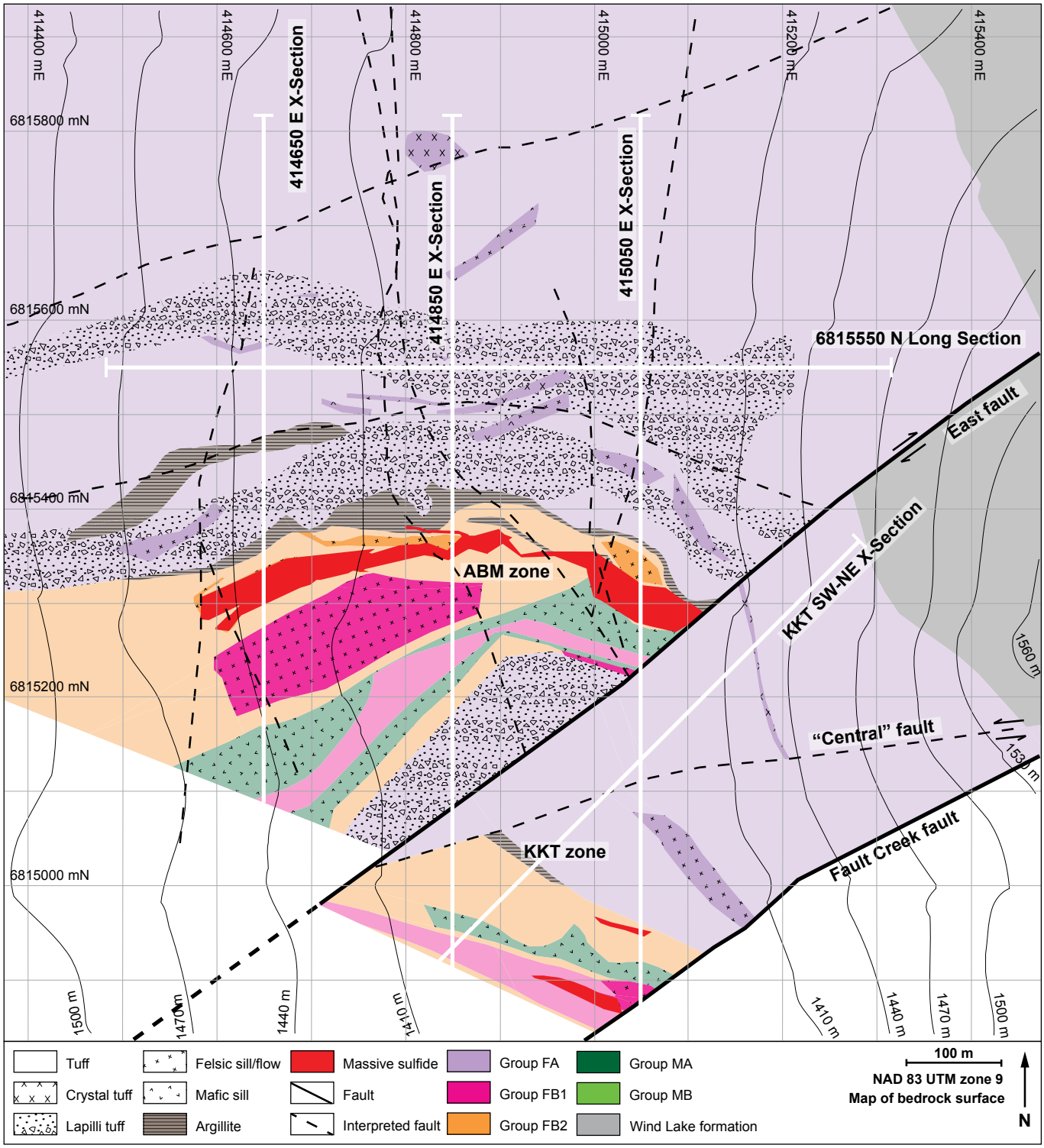

Fig. 3. Local geology of the ABM deposit. Map units constructed using drilling data and 3-D models of lithostratigraphic units, massive sulfide lenses, and interpreted faults. Displayed lines refer to long section in Figure 4 and cross sections in Figures 11 and 12. Note that lithofacies are displayed using patterns and geochemical groups using colors. Note: KKT zone = Krakatoa zone.

dominantly of felsic volcanic and subvolcanic rocks and mafic sills. At the upper contact, there is a single lens of argillite, defining the boundary with Sequence 3. Sequence 3 sits on top of Sequence 2 and is composed of interbedded lapilli tuff, crystal-rich tuff, tuff, argillite lenses, and felsic lava flows and sills. In the Krakatoa zone within Sequence 3, flows and sills are more common than in the ABM zone. Thin, fine-grained mafic sills commonly intrude Sequence 3.

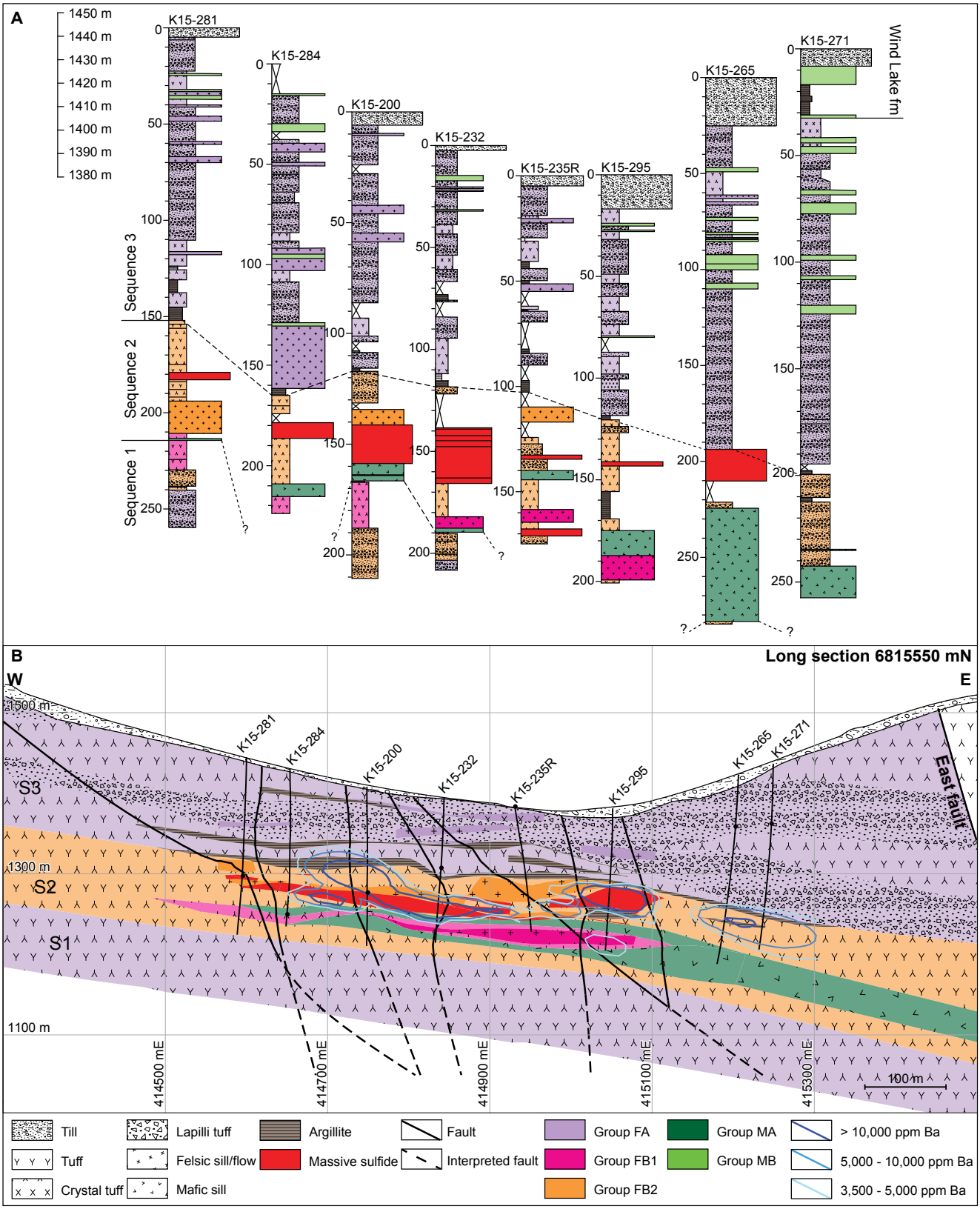

Fig. 4. Long section through the ABM zone of the ABM deposit with representative graphic logs. Section line position shown in Figure 3. (A) Drill hole collars are arranged according to elevation; drill hole depth adjusted for dip. (B) Long section running west to east, looking north. Drill holes are not clipped to section; entire extent of drill holes are displayed, and pierce points through section plane are marked. Abbreviations: FA = Felsic A, FB = Felsic B, and MA = Mafic A, S1 = Sequence 1, S2 = Sequence 2, S3 = Sequence 3.

Felsic volcaniclastic facies

Rocks of rhyolitic/dacitic composition occur within the volcano-sedimentary pile hosting the ABM deposit. Fabric in felsic volcaniclastic rocks is commonly defined by thin micaceous layers that are composed of thin white mica blades. These micaceous layers are up to 1 to 3 mm thick. Petrographic observations from less altered parts of the deposit suggest that the micaceous bands were at least partially formed by pervasive replacement of feldspar phenocrysts and subsequent recrystallization and deformation (Fig. 5A). Volcaniclastic rocks are commonly interbedded with each other and have transitional contacts between the different facies; graded bedding within tuffaceous layers is rare (Fig. 6A). Individual lapilli tuff lenses can be up to 70 m thick. Volumetrically minor sections of volcaniclastic rock show undulating foliation with minor scale folding (<0.5 m wavelength), commonly in association with argillite lenses or where the rocks are strongly altered. In the text below, the felsic volcaniclastic lithofacies are divided into further subfacies.

Tuff: Felsic tuffs are fine-grained to very fine grained with abundant thin white mica-rich layers that define the major fabric of the rock. Tuffs are typically moderately to poorly sorted and locally thinly to very thinly bedded (Fig. 6B) with only minor lapilli or feldspar crystals (Fig. 6C) occurring locally within the tuffs. The facies predominantly contains quartz, white mica, minor K-feldspar and plagioclase, minor carbonate, and trace disseminated pyrite. In thin section, quartz grains occur in lenses of similar grain size (Fig. 5B), with only minor mica and carbonate within these lenses/patches; white mica occurs between these lenses in bands that define the rock fabric.

Crystal-rich tuff: Felsic crystal-rich tuffs contain quartz and/or K-feldspar crystals within a tuffaceous matrix (Fig. 5C) that is fine-grained to very fine grained and contains quartz, white mica, minor K-feldspar and/or plagioclase, and minor carbonate. Quartz crystals are commonly rounded or subrounded, bluish in color, locally gray, up to 7 mm in diameter, and can compose up to 10 modal % of the rock (Fig. 6D). K-feldspar crystals are subhedral to euhedral, up to 30 mm in size, and can compose up to 40 modal % of the rock (Fig. 6E). Crystal-rich tuffs are commonly poorly sorted and transition gradually to non-crystal–rich tuffs, and lapilli tuffs locally transition to crystal-rich tuffs.

Lapilli tuff: Felsic lapilli tuffs consist of up to 60 to 80 modal % lapilli that are contained within a fine-grained to very fine grained tuffaceous matrix. White mica, quartz, minor K-feldspar and/or plagioclase, and local, trace disseminated sulfides compose the matrix. Lapilli fragments and the matrix are commonly flattened, exhibiting a well-defined structural fabric with the matrix consisting of very fine grained, white mica-rich layers (Fig. 6F). The rock fabric is locally gently to strongly folded. Lapilli fragments that are not flattened are commonly subangular. The lapilli are typically felsic and have a similar composition to the matrix (quartz-white mica). Locally, the lapilli are more altered than the matrix and are inferred to have originally been more porous, possibly even pumice clasts. The lapilli are locally altered to Fe carbonate, quartz, or pyrite and white mica. In some units, the lapilli tuffs contain lithic fragments/clasts with abundant chlorite-biotite, quartz patches, and minor Fe carbonate (Fig. 6G). Lapilli tuff units are commonly poorly sorted and massive but can grade into tuffs or crystal-rich tuffs.

Coherent felsic lithofacies

These lithofacies consist of aphyric rhyolite/dacite with only minor phenocrysts and are very fine grained. The lithofacies consist predominantly of quartz, minor white mica, K-feldspar, plagioclase, chlorite, and trace sulfides. Rarely, K-feldspar porphyritic textures are present, with euhedral K-feldspar phenocrysts up to 30 mm in size comprising up to 5 modal % of rock. The rocks are gray-white to beige-buff in color, but are locally orange, and rarely pink (Fig. 6H). Locally, aphyric rhyolite/dacite displays flow banding (Fig. 6I) or contains quartz-filled amygdales. Contacts with surrounding rocks can be sharp, but commonly the margins consist of flattened hyaloclastite (Fig. 6K). Locally, perlitic fracturing (Fig. 6J) occurs on contacts. Units with hyaloclastite or brecciation on contacts, and/or with flow banding and amygdales, indicate deposition on the sea floor or at very shallow depths below the sea floor as individual flows (McPhie et al., 1993). We interpret these units as flows; they have aspect ratios between 1:2.5 and 1:4 and occur within all three sequences. The units with mostly sharp contacts and coherent interiors are interpreted to have been emplaced as subvolcanic sills (Gibson et al., 1999) and have aspect ratios ~1:1.5. The coherent interior of the sills is typically fractured with quartz veinlets with associated carbonate, biotite, and/or sulfides.

Mafic sills

Sills in Sequence 2: In the ABM zone, mafic subvolcanic rocks are present as two main sills with a relatively uniform thickness (~10 m) that increases towards the east of the ABM zone (max. thickness 40 m). The Krakatoa zone contains one main sill with varying thickness (20–100 m) and three minor sills protruding from the main body. In both zones, the mafic sills occur in Sequence 2, where they intrude the volcano-sedimentary pile and are emplaced along contacts of a preexisting felsic sill. In the eastern part of the ABM zone, the lower mafic sill crosscuts the pre-existing felsic sill. The mafic sills have chilled margins that are fine- to medium-grained (Fig. 6L) and gradually transition to coarser grain sizes in the interior of the sills, where clumps of amphibole occur within the fine-grained groundmass (Fig. 6M). The sills consist of minor primary pyroxene and plagioclase and contain alteration minerals including amphibole, biotite, chlorite, carbonate, epidote, K-feldspar, white mica, and minor quartz that replace 90 to 95% of the primary minerals. The finer-grained contacts of the sills are more strongly altered relative to the interiors of the sills where chlorite-carbonate alteration occurs with disseminated biotite. Euhedral-subhedral pyrrhotite-pyrite composite grains up to 2.5 cm in size occur within the coarse-grained parts of the sills.

Sills in Sequence 3: Thin mafic sills occur predominantly in the hanging wall of the massive sulfide lenses, commonly in Sequence 3 below the lower Wind Lake formation contact. The sills have sharp contacts and are commonly emplaced bedding-parallel to the felsic volcaniclastic rocks (Fig. 6N). Locally, the sills crosscut the bedding at a low angle. They are dark green or buff in color and are commonly fine- to very fine grained and massive. Their thickness is commonly between 10

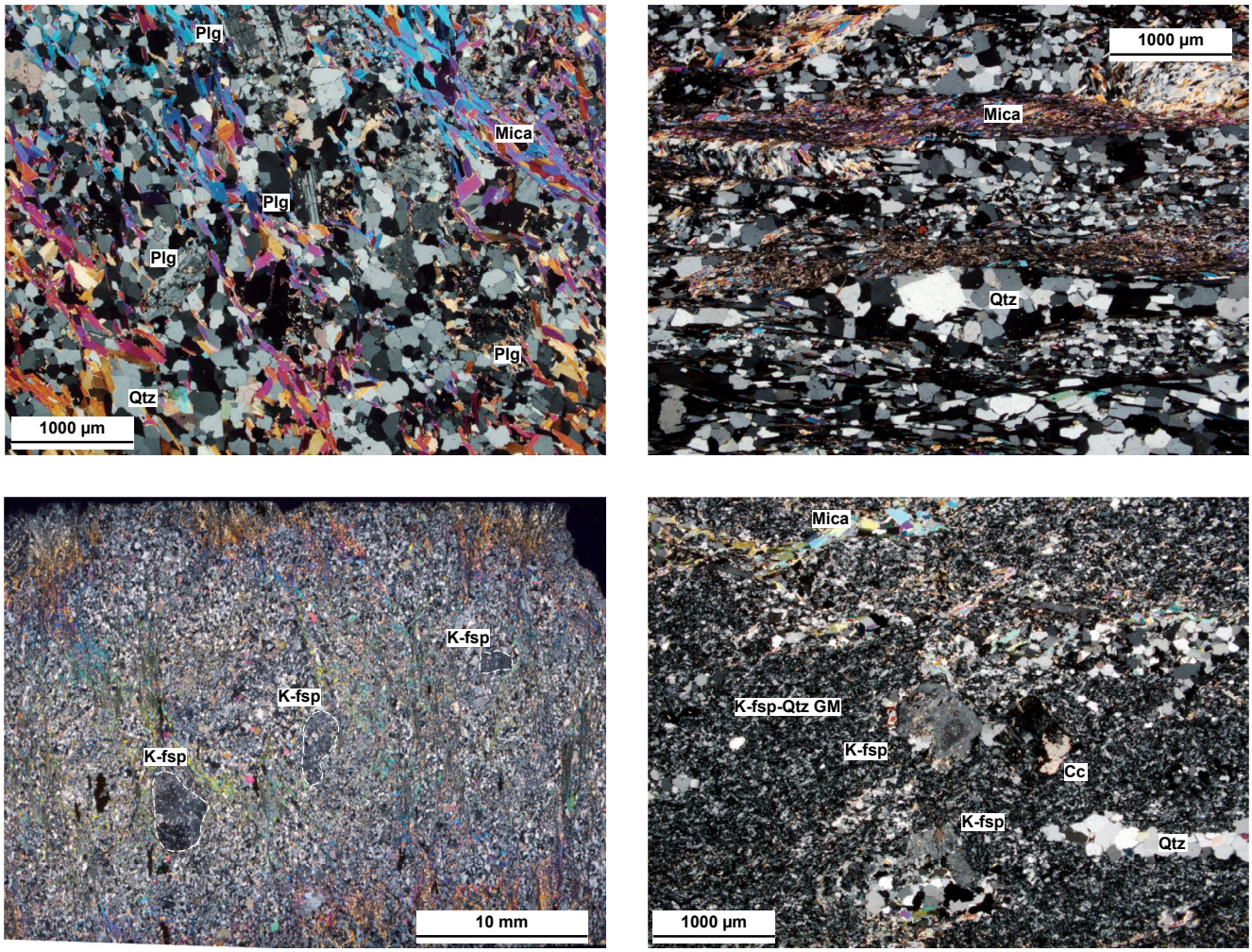

Fig. 5. Microscopic textures preserved in host rocks from the ABM volcanogenic massive sulfide (VMS) deposit. (A) Groundmass of crystal-rich tuff; plagioclase grains are weakly to moderately sericitized and overprinted by later white mica fabric; K15-233, 108.1 m downhole. (B) Matrix of lapilli tuff; lenses composed of quartz grains of varying grain size; fine-grained mica fabric in between lenses; K16-370, 277 m down hole. (C) Large K-feldspar crystals, partially sericitized in fine-grained quartz–K-feldspar matrix; later white mica bands overprinting matrix; K15-260, 57.1 m downhole. (D) Felsic lava flow with preserved very fine grained groundmass consisting of quartz–K-feldspar with preserved K-feldspar phenocrysts that are moderately sericitized and overprinted by calcite; minor later white mica replacing coarser quartz and K-feldspar grains; K15-315, 151.65 m downhole. Abbreviations: Cc = calcite, K-fsp = K-feldspar, Mica = white mica, Plg = plagioclase, Qtz = quartz.

cm and 1 m, but can be up to 2.5 m and locally, in rare cases, can be up to 8.5 m. Chlorite and biotite alteration is common, as are overprinting carbonate, quartz, and quartz-carbonate veins.

Sedimentary facies

Argillite: Carbonaceous argillite lenses are very fine-grained and thinly bedded (Fig. 6O). Dark gray to black argillite beds are intercalated with minor tuffaceous or carbonate-rich beds. Locally, minor pyrite and/or pyrrhotite occur. Argillite lenses up to 1 m thick are interbedded with tuff, lapilli tuff, or crystal-rich tuff. The argillite units are commonly strongly foliated, locally crenulated, and/or pervasively quartz altered. Strong foliation and crenulation are likely due to different rheological behavior of the argillite compared to the volcaniclastic and volcanic rocks. Folded quartz and/or quartz-carbonate veins that overprint the argillite fabric are common.

Faults

A set of NE-SW–striking (azimuth 050°–060°) subvertical to vertical regional faults cuts the stratigraphy in the deposit area. The two major faults crosscutting the ABM deposit are the East fault and the Fault Creek fault (Fig. 3); these two faults define the Krakatoa block. Movement on the East fault was dextral-oblique with roughly 200 m of apparent offset; van Olden et al. (2020) interpret the Krakatoa block as dropped to the northwest and rotated. Fault rock within both the major fault zones contains angular sulfide clasts along with clay-sized fault gouge, indicating the movement and offset on the faults occurred postmineralization. A lesser order fault, running east-northeast–west-southwest (~080°) and terminating on the East and Fault Creek faults, bisects the Krakatoa block ("Central" fault; Fig. 3). The fault is subvertical and dextral and accommodated a lateral offset of ~100 m after the forma-

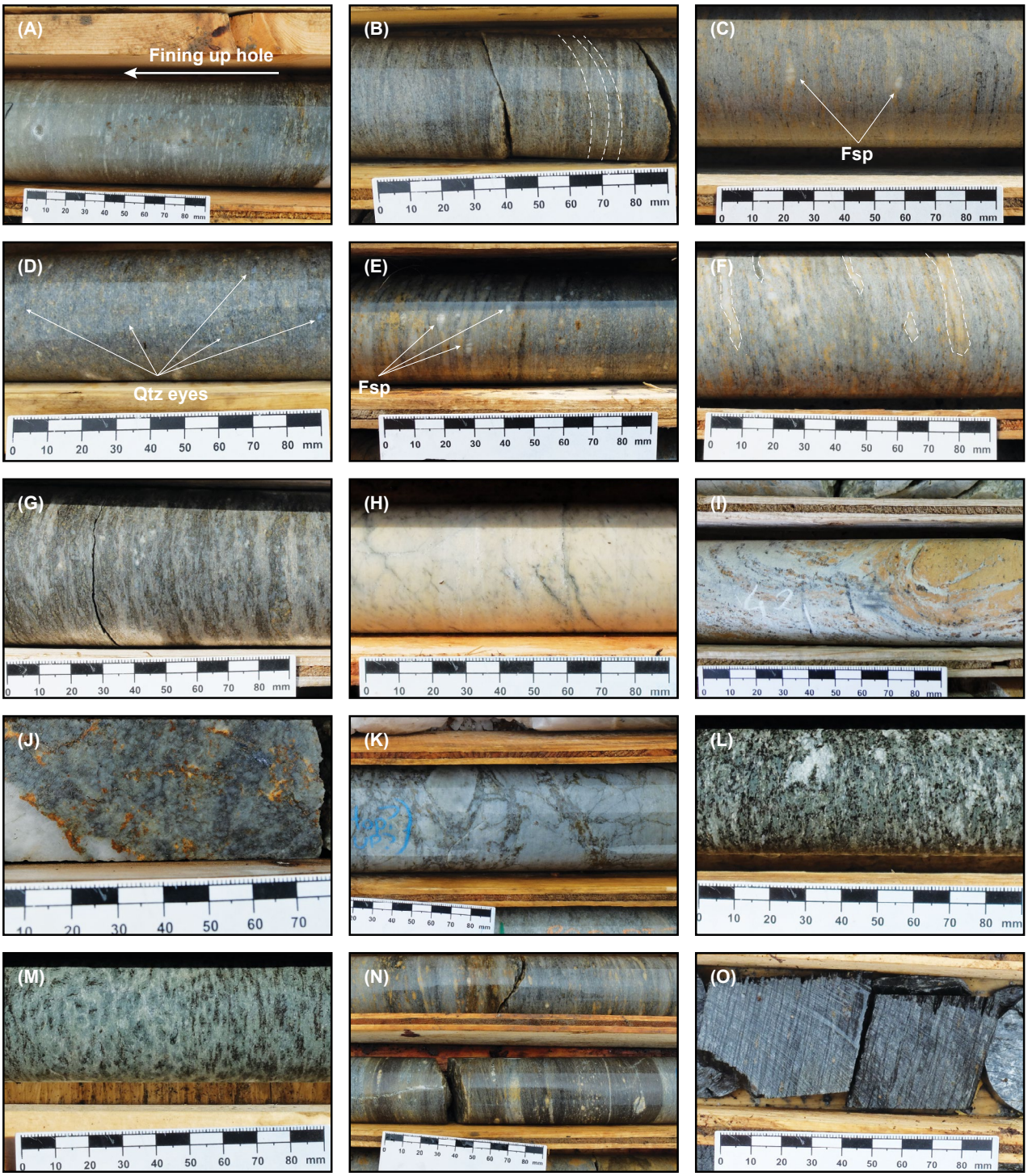

Fig. 6. Lithofacies present at the ABM deposit. (A). Graded bedding in felsic tuff, arrow showing direction of fining uphole; K18-484, 37 m down hole. (B) Felsic tuff; K15-291, 41 m down hole. Bedding marked by dashed line. (C) Felsic tuff with minor feldspar crystals, arrows pointing to feldspar grains; K15-216, 72 m downhole. (D) Crystal-rich tuff with blue quartz eyes, arrows point to examples of the quartz eyes; K15-206, 62 m down hole. (E) Crystal-rich tuff with feldspar crystals, arrows point to examples of feldspar crystals; K15-233, 81 m downhole. (F) Lapilli tuff, examples of lapilli highlighted by dashed line K15-260, 58 m downhole. (G) Lapilli tuff, fragments with blue quartz eyes, minor feldspar crystals, and biotite-Fe carbonate alteration; K15-260, 204 m downhole. (H) Aphyric rhyolite; K15-251, 63 m downhole. (I) Flow banding in aphyric rhyolite; K15-231, 42 m downhole. (J) Perlitic fracturing in rhyolite; K15-236, 94 m downhole. (K) Jigsaw breccia on top of rhyolite flow; K16-358, 85 m downhole. (L) Fine-grained and strongly altered lower contact of a Mafic A (MA) mafic sill from Sequence 2; K15-265, 267 m downhole. (M) Coarse-grained interior of MA mafic sill from Sequence 2; K15-265, 254 m downhole. (N) Thin Mafic B (MB) mafic sill from Sequence 3; K15-232, 61 m downhole. (O) Argillite; K15-301, 70 m downhole. Abbreviations: Fsp = feldspar, Qtz = quartz.

tion of the mineralization, since it does not contain any sign of replacement or vein mineralization within the fault fabric. The thickening of subvolcanic units in the Krakatoa zone and their relative abundance compared to the ABM deposit suggests that the East fault or its predecessor was likely present and acted as a feeder/conduit for the ascending magmas. The mafic sills present at Krakatoa unify into a single body and considerably thicken (up to 150 m) north of the "Central" fault. The single body takes on a more dike-like morphology and it parallels the East fault (van Olden et al., 2020). The East fault was later reactivated and facilitated the offset of the Krakatoa zone. The Fault Creek fault and the lower order fault with lateral offset ("Central" fault) do not appear to have controlled coherent rock emplacement or unit thickness.

Mineralization

The ABM VMS deposit consists of two mineralized zones: the ABM zone and the Krakatoa zone (Fig. 3). The mineralization is stratabound in both zones, subcrops at the bedrock surface below the till cover, and dips subparallel to the stratigraphy (20°–30°). The ABM zone extends 700 m along strike and goes from the bedrock surface downdip for 600 m. The Krakatoa zone measures 170 m along strike and extends from the bedrock surface downdip for 600 m and remains open downdip. In both zones, the mineralization occurs as a series of stacked lenses within Sequence 2 rocks and ranges in thickness from 5 to 55 m in the ABM zone and from 15 to 100 m in the Krakatoa zone. Mineralization in the ABM zone tapers off downdip to the north-northeast, laterally to the west, and is cut off by the East fault to the east. In the Krakatoa zone, mineralization thins out downdip to the northeast and is cut off by postmineralization faults in other directions (Fig. 11,12).

In both the ABM and Krakatoa zones, massive sulfide mineralization is composed of pyrite, sphalerite, and pyrrhotite, with lesser chalcopyrite, magnetite, and galena and minor tennantite-tetrahedrite and freibergite. The most common gangue minerals are barite, carbonate, quartz, chlorite, and white mica. Three main mineralization assemblages compose the massive sulfide lenses: (1) pyrite-sphalerite-galena with lesser chalcopyrite, tennantite-tetrahedrite, and freibergite, with carbonate, barite, quartz, and white mica (Fig. 7A-D); (2) magnetite-chalcopyrite-pyrrhotite-pyrite-sphalerite, minor tennantite-tetrahedrite and freibergite, and minor carbonate and chlorite (Fig. 7E); (3) chalcopyrite-pyrrhotite-pyrite stringers associated with pervasive chlorite alteration, minor carbonate, and quartz (Fig. 7F). The massive sulfide lenses are primarily composed of the first two assemblages. The third assemblage is not as common and typically only present at the upper and lower contacts of the massive sulfide lenses. The latter two assemblages are richer in chalcopyrite, magnetite, and chlorite, are indicative of higher temperatures of emplacement (>300°C; e.g., Lydon, 1988), and are interpreted to have formed earlier than the pyrite-sphalerite-galena assemblage.

Mineralization at the ABM deposit has generally sharp contacts, but locally grades into unmineralized but altered rocks over the distance of 1 to 2 m. In the ABM zone, massive sulfide mineralization is associated primarily with felsic volcanic and volcaniclastic rocks. In the Krakatoa zone, the majority of massive sulfide mineralization is localized on contacts between the mafic sills and volcaniclastic rocks or, locally, within the

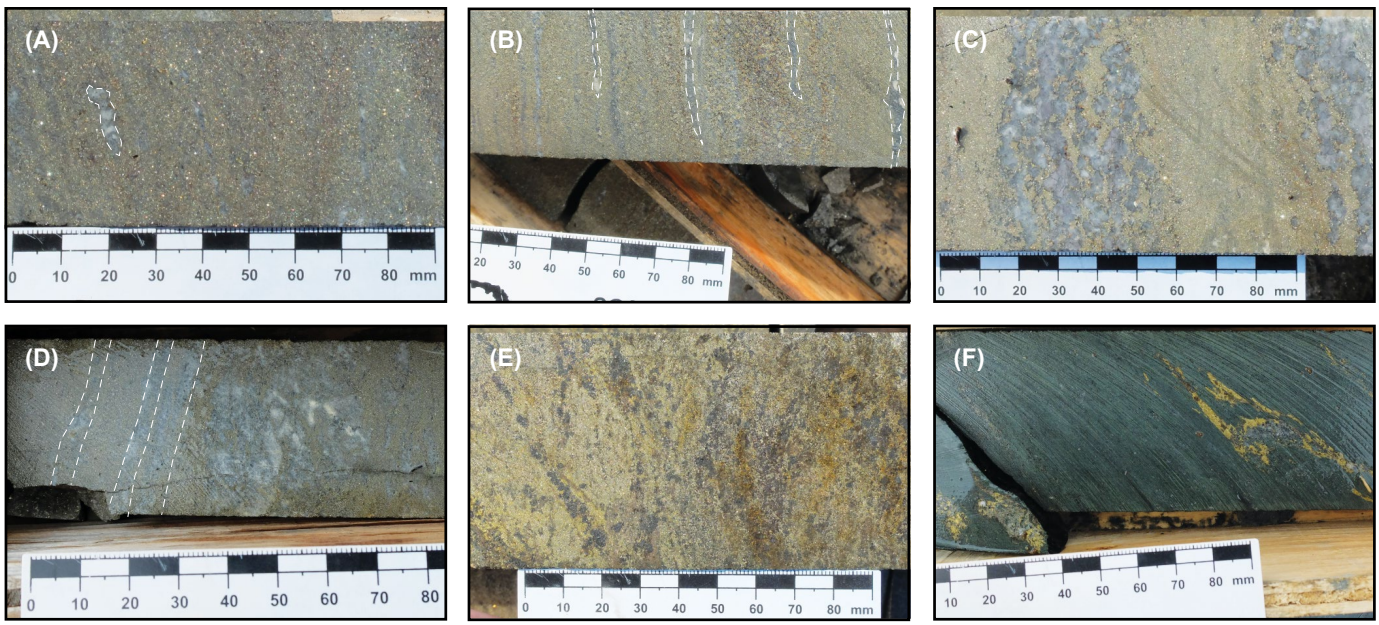

Figure 7. Mineralization textures present at the ABM deposit. (A) Massive py ± sph with remnant clasts, clast highlighted with dashed line; K15-265, 185 m downhole. (B) Massive py-sph with remnant lapilli clasts with quartz crystals; clasts are white mica-chlorite altered and highlighted with dashed line; K15-274, 92 m downhole. (C) Massive py ± sph ± cpy replacing felsic flow along perlitic fractures; K15-200, 143 m downhole. (D) Massive py-bar with remnant bedding visible; bedding highlighted with dashed line; K15-286, 139 m downhole. (E) Massive py-po-mgt-cpy mineralization; K12-200, 149 m downhole. (F) Pervasive chlorite alteration with cpy-po stringers; K17-422, 153 m downhole. Abbreviations: bar = barite, cpy = chalcopyrite, mgt = magnetite, po = pyrrhotite, Py = pyrite, sph = sphalerite.

mafic sills themselves. Throughout the ABM deposit, features such as preserved lapilli and other clasts (Fig. 7A-B), remnant bedding (Fig. 7D), and massive sulfides replacing likely glassy groundmass within perlitic and brecciated textures on unit contacts (Fig. 7C) are observed within the massive sulfide lenses and on their contacts and suggest that the mineralization formed by replacement (Doyle and Allen, 2003).

Thin, discontinuous stratiform bands (<30 cm thick) of massive sulfide occur in the footwall of the major massive sulfide lenses within the volcaniclastic rocks of Sequence 2 and at the top of Sequence 1. In the hanging wall of the massive sulfide lenses, rare subrounded to subangular clasts (up to 30 cm in size) composed of pyrite-pyrrhotite-carbonate occur within the felsic volcaniclastic rocks of Sequence 2 and Sequence 3.

Alteration

Hydrothermal alteration is widespread both in the hanging wall and footwall of the massive sulfide mineralization in the ABM and Krakatoa zones. The extent and zonation of alteration assemblages is irregular, although the intensity of alteration increases with proximity to the mineralized lenses. Alteration assemblages can vary within a single unit; however, white mica ± quartz ± chlorite alteration is the most widespread assemblage in felsic rocks. Felsic volcaniclastic rocks and lavas commonly display pervasive white mica alteration at the contacts of massive sulfide lenses, but locally, pervasive chlorite ± carbonate alteration occurs. Carbonate (i.e., calcite, dolomite, and ankerite) is a common constituent of alteration assemblages at both the ABM and Krakatoa zones, and occurs within the massive sulfides, in proximity to mineralization, or in more distal parts of the deposit. Calcite, dolomite, and Fe carbonate alteration is widespread in Sequences 2 and 3, and commonly presents as patches or veins with an orange tint. They commonly overprint the primary fabric and/or the mineralization. Amphibole-chlorite-carbonate-biotite-epidote-quartz are common alteration minerals in the altered mafic subvolcanic sills in Sequence 2, where amphibole and chlorite replace the primary pyroxene and biotite overprints the chlorite locally. Postmineralization carbonate, carbonate-quartz, quartz, quartz-tourmaline, and tourmaline veins occur throughout the deposit and crosscut the rock fabric defined by the primary features in the volcaniclastic rocks and the mineralization.

Lithogeochemistry

Whole-rock major and trace element lithogeochemistry methods

Eighty-three of the collected samples were analyzed for major and trace elements; the full results are available in Appendix Table A1. Sample preparation and measurement of major and trace element data was performed at ALS Laboratories, North Vancouver, British Columbia. Rock samples were crushed and pulverized using steel plates and agate mills, respectively. Sample powders (~0.2 g) were fused with a lithium metaborate flux (0.9 g) at 1,000°C. The fused beads were cooled and digested using 100 mL of a 4% HNO_3-2% HCl mixture. Analyses of the sample solutions were carried out using inductively coupled plasma-atomic emission spectrometry (ICP-AES) for major elements and inductively coupled plasma-mass spectrometry (ICP-MS) for trace elements. Additional trace element measurements were completed on the same sample suites at Ontario Geoscience Laboratories in Sudbury, Ontario, to obtain transition metals, base metals, and semimetals (e.g., Li, Be, Co, Cu, Zn, Mo, Cd, In, Sb, W, Bi, Pb, Sc, Ta). Samples were digested on hot plates using a mixture of HF-HCl-$HClO_4$ in closed screwcap Savillex® Teflon™ bombs for seven days. The resultant solution was dried down and fluxed with a dilute HCl-$HClO_4$ mixture and reheated. Samples were again dried down and fluxed with a final mixture of concentrated HNO_3-HCl, heated, and finally diluted with HNO_3. Solutions were analyzed for metals on a Perkin-Elmer Elan 9000 ICP-MS following the methodology of Burnham and Schweyer (2004) and Burnham (2008).

Over the course of this study, eight in-house reference materials (SLV-MC basalt and WP-1) and five lab-chosen duplicates were analyzed at ALS and Ontario Geoscience Laboratories during the run to monitor analytical accuracy and reproducibility (App. Table A2). The SLV-MC basalt and WP-1 dacite (Watts Point, Coast Plutonic Complex) samples were reproducible to <5% for major elements, except for <10% MnO in the WP-1 dacite. Trace element concentrations overall gave relative standard deviation (RSD) values <10%, with many elements below 5%, except for Hf and Lu (<12%) in both reference materials, and Cs and V in SLV-MC (App. Table A2). The results for both reference materials overlap with published values (WP-1; Piercey et al., 2001; Manor and Piercey, 2019) and unpublished in-house data for both SLV-MC (n = 44) and WP-1 (n = 19) with reproducibility better than 15% for most trace elements and major element oxides, with the exceptions of Cs and Tl in SLV-MC basalt, which show percent relative differences <61%, and Be, Co, Cs, Mo, Ni, Sb, Sc, Sn, and Tl in the WP-1 dacite, which show percent relative differences >100%. The high percent relative difference values for the trace elements in the WP-1 dacite standard are likely due to a low number of analyses available for the analytes in question in the internal standard for the analytical method used in this paper (n = 4). The lab-chosen duplicates show relatively higher RSD values but are generally <15% for most major and trace elements.

Lithogeochemical results

The 83 analyzed samples cover the stratigraphic interval hosting the ABM deposit and encompass rocks from Sequence 1 approximately 60 m below the massive sulfide mineralization to rocks from Sequence 3 below the contact with the Wind Lake formation (Fig. 4). Samples commonly contain alteration minerals such as white mica, chlorite, carbonate, quartz, and Fe sulfides (pyrite and pyrrhotite). Examination of the major element data shows that the majority of the sampled rocks were affected by hydrothermal alteration (Fig. 8B; Spitz and Darling, 1977; Barrett and MacLean, 1994; Large et al., 2001b; Ruks et al., 2006). Most felsic samples have elevated loss on ignition (LOI) values (>2 wt %; Le Maitre et al., 1989) and Al_2O_3/Na_2O values (2.2–401, n = 64) indicative of feldspar destruction or replacement by white mica (Spitz and Darling, 1977; Ruks et al., 2006). Iron carbonate and carbonate alteration can lead to the distortion of expected CaO behavior. Commonly, the majority of primary CaO is lost due to destruction of plagioclase and its replacement by white mica and chlorite,

but strongly carbonate-altered samples show significant additions of CaO. The high degree of hydrothermal alteration (Fig. 8B) precludes the use of the mobile major elements for characterization of lithological units. Rare earth elements (REEs), high field strength elements (HFSEs), Al_2O_3, and TiO_2 are immobile under most VMS conditions (Kranidiotis and MacLean, 1987; MacLean, 1988; MacLean and Barrett, 1993). The immobile behavior of REE-HFSE-Al_2O_3-TiO_2 was assessed and confirmed using methods outlined in MacLean (1988) and MacLean and Barrett (1993). Immobile elements (Zr, TiO_2, Al_2O_3, REEs, Cr, Hf, Nb, Sc, Ta, Th, V, and Y) and their ratios are thus used to determine and characterize distinct lithogeochemical groups within the ABM deposit stratigraphy. Values for representative samples and median values for each group in both the ABM and Krakatoa zones are presented in Table 1. Lithogeochemical results confirm the bimodal nature of the volcanic rocks; these are visible on the Zr/Ti vs. Nb/Y plot, where all samples plot either as basalt or dacite/trachyte (Fig. 8A).

Felsic rocks: Immobile element ratios illustrate there are two distinct groups of felsic rocks, FA, and FB, in the ABM deposit stratigraphy (Fig. 8D). Both groups occur both as coherent and volcaniclastic lithofacies, which indicates the signatures are not controlled by lithology alone. Groups FA and FB plot on the same linear array in the Zr-TiO_2 space (Fig. 8C), but plot on distinctly different linear arrays that pass through the origin in the Al_2O_3/TiO_2-Zr/Al_2O_3 space (Fig. 8D).

Group FA: In Nb/Y-Zr/Ti space (Fig. 8A), group FA rocks plot in the trachyte field with a minor portion overlapping into the dacite-rhyolite field. Group FA rocks have relatively high absolute values of Zr (Zr > 548 ppm, n = 20) compared to the other felsic rocks in the Kudz Ze Kayah formation and overall higher values of HFSEs like Hf, Nb, Sc, V, and Y compared to other felsic rocks (Table 1). The Zr/TiO_2 ratio varies between 1,046 and 1,367, and Zr/Al_2O_3 is between 40.6 and 52.9. The Zr/Y ratio for all samples of group FA are >10 (10.8–16.4; Fig. 8E), indicative of subalkaline to alkaline affinity (Ross and Bédard, 2009). In the Nb-Y plot, the group FA rocks fall into the within-plate affinity field (Fig. 8F; Pearce et al., 1984). The primitive mantle (PM) normalized La/Yb ratio of $((La/Yb)_{PM})$ is between 9.4 and 15.9, indicating steep REE pattern slopes where light rare earth elements (LREEs) are enriched relative to the heavy rare earth elements (HREEs) and the HREEs display a relatively flat pattern (Fig. 9B). The mean Eu anomaly (Eu/Eu*) for group FA rocks is around 0.53 (n = 20). In extended PM-normalized plots, Nb and Ti show negative anomalies compared to Th and La and Eu and Gd, respectively (Fig. 9A); the mean Nb/Ta value is 17.56 (n = 13). In felsic volcanic fertility diagrams (Fig. 9D), group FA rocks plot mostly outside of the designated fields near the border between the FI and FII rhyolite fields.

Group FB: In the Nb/Y-Zr/Ti discrimination diagram, group FB rocks plot in the rhyolite-dacite field, and a small portion overlaps into the trachyte field (Fig. 8A). Group FB rocks have absolute Zr concentrations between 157 and 507 ppm (n = 38), relatively lower values of HFSEs compared to the FA group (Table 1), and the Zr/TiO_2 and Zr/Al_2O_3 values range from 907 to 1,340 and 12.7 to 31.4, respectively. The Zr/Y values for all samples of group FB are slightly lower than group FA rocks and vary between 2.6 and 16.1 (mean = 7.3; Fig. 8E), indicative of a calc-alkaline affinity (Ross and Bédard, 2009). In the Nb vs. Y diagram, the rocks of group FB fall into the within-plate affinity field (Fig. 8F), but some samples plot close to the syncollisional and volcanic arc fields. The FB group can be further divided into subgroups FB1 and FB2 based on immobile elements and their ratios. The FB1 subgroup has the higher average Zr (400 ppm, n = 15) and TiO_2 (0.32 wt %, n = 15) values of the FB group. The FB group typically contains tuffaceous or sill lithofacies; lapilli or crystal-rich tuffs are rare. Subgroup FB1 typically occurs associated with group MA mafic subvolcanic sills. The FB2 subgroup is the most common lithogeochemical signature in the ABM sample suite and encompasses all observed lithofacies. The $(La/Yb)_{PM}$ of the FB group falls between 4.4 and 14.1, indicating a similar to slightly flatter REE slope than group FA, and samples from both subgroups have similar chondrite-normalized REE patterns (Fig 9B). The LREEs are rich relative to the HREEs, and the HREEs have relatively flat patterns, similar to group FA but with relatively lower abundances (Fig. 9B). The mean Eu anomaly (Eu/Eu*) for subgroup FB1 rocks is 0.25 (n = 15) and 0.19 (n = 23) for subgroup FB2. The FB group rocks show negative Nb and Ti anomalies (Fig. 9A) similar to the FA group but have a lower mean Nb/Ta value for the group that is 12.40 (N = 27). In the felsic volcanic fertility diagram (Fig. 9D), group FB rocks plot within the FII rhyolite field.

Mafic rocks: Mafic rocks in the uppermost 350 m of the Kudz Ze Kayah formation occur in two distinct geochemical groups: (1) group Mafic A (MA), which comprises the mafic sills in Sequence 2; and (2) group Mafic B (MB), which consists of the sills in Sequence 3. The two groups differ not only in their stratigraphic position, but also in their immobile and trace element signatures.

Group MA: Group MA rocks plot in the basalt field in Nb/Y-Zr/Ti space (Fig. 8A). Values of Zr are between 78 and 111 ppm (n = 16), TiO_2 falls between 1.06 and 1.51 wt % (n = 16), and P_2O_5 values are between 0.11 and 0.17 wt % (n = 16). The Zr/TiO_2 values fall between 63.0 and 80.5 (n = 16), and the Zr/Y values are between 4.0 and 5.6 (Fig. 8E), straddling the line between transitional and calc-alkaline affinity (Ross and Bédard, 2009). The mean Nb/Ta value is 16.49 (N = 5). In several discrimination diagrams (Pearce and Cann, 1973; Pearce, 1996, 2008), group MA plots in the fields designated for enriched mid-ocean ridge basalts (E-MORBs) and within-plate tholeiites (WPT; Fig. 10B-D), for MORB (Fig. 10A), or near the within-plate basalt (WPB)/calc-alkali basalt (CAB) field (Fig. 10B). In a PM-normalized plot, group MA has a relatively smooth downward sloping curve with a slight negative Nb anomaly in comparison to Th and La (Fig. 9C; Nb/Nb* average 0.81, n = 16). The $(La/Yb)_{PM}$ ratio is between 2.83 and 3.72 and indicates a relatively flat REE slope (Fig. 9C).

Group MB: In Nb/Y-Zr/Ti space, the group MB samples plot in the basalt field (Fig. 8A). Values of Zr are between 195 and 349 ppm (n = 6), TiO_2 is between 2.00 and 2.93 wt % (n = 6), and P_2O_5 values are between 0.28 and 0.39 wt % (n = 6). The Zr/TiO_2 value falls between 94.0 and 119.1 (n = 6); the Zr/Y value is between 5.6 and 14.0 and plots in the calc-alkaline affinity field (Ross and Bédard, 2009; Fig. 8E). The mean Nb/Ta value is 15.90 (N = 2). In several discrimination diagrams (Pearce and Cann, 1973; Pearce, 1996, 2008), group MB plots in the fields designated for WPBs and volca-

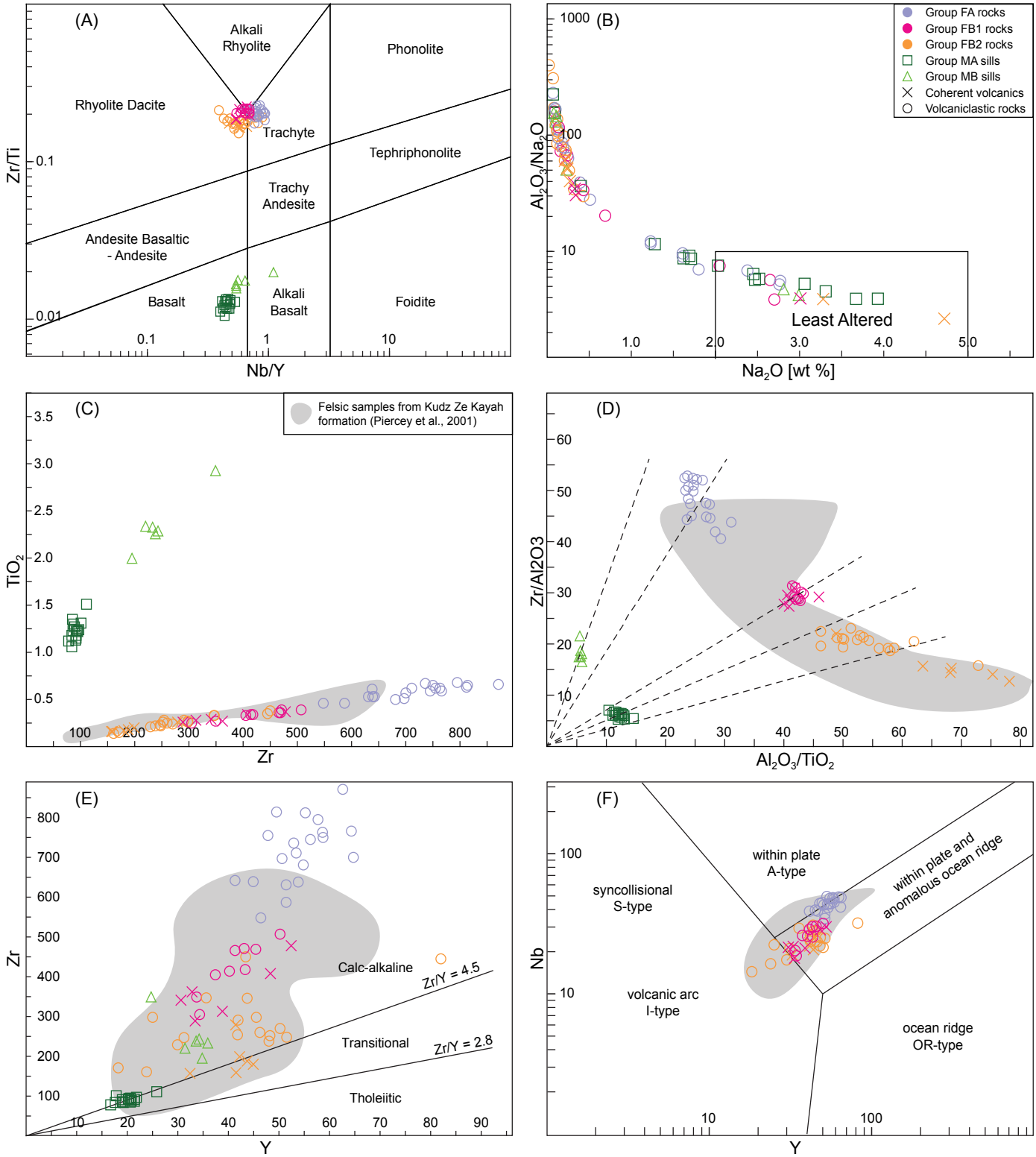

Fig. 8. Trace and major element discrimination plots for felsic and mafic rocks in the ABM deposit. (A) Volcanic rocks discrimination diagram, Nb/Y vs. Zr/Ti (Pearce, 1996). (B) Na_2O vs. Al_2O_3/Na_2O showing least altered rocks (Ruks et al., 2006). (C) Zr vs. TiO_2. (D) Al_2O_3/TiO_2 vs. Zr/Al_2O_3 (Barrett et al., 2001). (E) Y vs. Zr (Ross and Bédard, 2009). (F) Y vs. Nb (Pearce et al., 1984). Gray shaded areas represent felsic samples from the Kudz Ze Kayah formation presented in Piercey et al. (2001). Abbreviations: FA = Felsic A, FB = Felsic B, MA = Mafic A, MB = Mafic B.

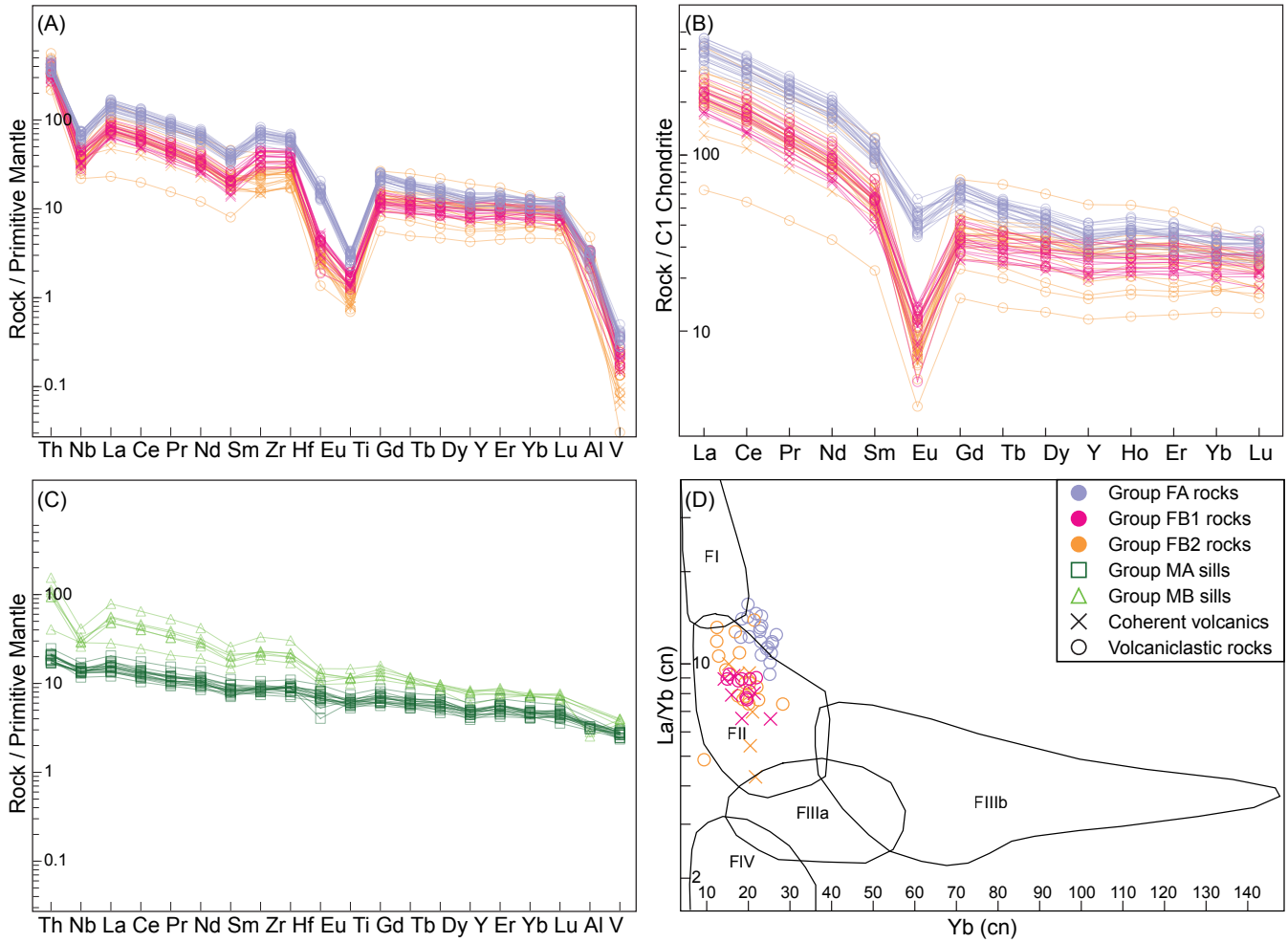

Fig. 9. Normalized plots of immobile and rare earth elements of the rocks from the ABM deposit. (A) Immobile elements of felsic samples normalized by primitive mantle (McDonough and Sun, 1995). (B) Rare earth elements of felsic samples normalized by C1 chondrite (McDonough and Sun, 1995). (C) Immobile elements of mafic samples normalized by primitive mantle (McDonough and Sun, 1995). (D) Chondrite-normalized felsic samples in plot distinguishing FI-FIV geochemical groups (Lesher et al., 1986; Hart et al., 2004). Symbols same as in Figure 8. Abbreviations: FA = Felsic A, FB = Felsic B, MA = Mafic A, MB = Mafic B.

nic arc basalts (VABs) and CABs (Fig. 10B-D) or straddles the line between MORB and ocean island basalt (OIB) (Ti/V = 41.3–57.4, n = 6; Fig. 10A). In a PM-normalized plot, group MB curves are downward sloping with a significant negative Nb (Nb/Nb* avg 0.48, n = 6; Fig. 9C) and a slight Ti anomaly, while the $(La/Yb)_{PM}$ ratio falls between 3.78 and 10.74. Group MB has similar geochemical characteristics to group 4b in Piercey et al. (2002b) and to the Wind Lake formation mafic rocks presented in Manor and Piercey (2019; Fig. 10).

Chemostratigraphy

Distribution of the various lithogeochemical groups in the upper Kudz Ze Kayah formation is described below from stratigraphically lowest to highest based on representative sections of the ABM and Krakatoa zones. In the 6815550 mN long section (Fig. 4), the 414650 mE, 414850 mE, and the 414050 mE cross sections through the ABM zone (Fig. 11), and the presented Krakatoa cross section (Fig. 12), the chemostratigraphy is similar between the two zones. However, the Krakatoa zone shows minor differences compared to the ABM zone, which are described below. Where geochemical sampling is lacking, units are inferred based on spatial extent of defined lithogeochemical groups. The lithogeochemical database of BMC Minerals Ltd. was also utilized, but only as a secondary source of major and trace element data.

Sequence 1: At the top of Sequence 1, a felsic volcanic unit with thickness varying between 3 and 25 m sits below the lower mafic sill and comprises felsic tuffs and volcanic rocks with FB1 signatures (Fig. 4). The felsic volcanic and volcaniclastic rocks sitting below the FB1 unit make up the majority of the stratigraphy in Sequence 1 and belong to the FA lithogeochemical group.

Sequence 2: Close to the lower contact of Sequence 2, the felsic subvolcanic sills, domes, and minor associated tuffs have group FB1 signatures. The two mafic sills occurring at the lower contact of Sequence 2 belong to the MA lithogeochemical group. Felsic rocks occurring in Sequence 2 below the Sequence 3-Sequence 2 boundary belong to the FB group. The boundary between Sequence 3 and Sequence 2 is sharp and coincides with the transition between FA rocks

Table 1. Summary of Geochemical Characteristics of the Rock Groups of the Upper Kudz Ze Kayah Formation

	FA			FB1			FB2			MA			MB		
	N	Mean	2σ	N	Mean	2σ	N	Mean	2σ	N	Mean	2σ	N	Mean	2σ
SiO_2	20	65.22	2.27	15	72.09	3.53	23	68.84	13.07	16	44.73	1.99	6	47.12	4.78
Al_2O_3	20	14.89	1.16	15	13.58	1.97	23	13.45	2.86	16	14.93	0.65	6	13.29	1.38
Fe_2O_3	20	4.50	1.45	15	2.18	1.12	23	3.67	5.33	16	9.53	0.59	6	10.87	0.84
CaO	20	2.41	0.96	15	1.37	0.95	23	1.76	2.50	16	9.52	1.32	6	7.40	2.34
MgO	20	1.57	0.45	15	0.50	0.36	23	2.69	3.32	16	7.76	0.84	6	3.09	0.37
Na_2O	20	0.88	0.93	15	0.90	1.05	23	0.52	1.10	16	1.90	1.23	6	1.05	1.31
K_2O	20	4.42	0.86	15	6.36	2.64	23	4.19	1.80	16	2.04	1.65	6	4.02	1.93
TiO_2	20	0.58	0.07	15	0.32	0.05	23	0.24	0.06	16	1.23	0.10	6	2.36	0.28
MnO	20	0.09	0.04	15	0.03	0.02	23	0.05	0.05	16	0.14	0.01	6	0.17	0.02
P_2O_5	20	0.18	0.02	15	0.04	0.01	23	0.04	0.02	16	0.13	0.02	6	0.35	0.03
LOI	20	4.66	1.00	15	2.62	0.98	23	4.62	4.06	16	7.24	3.02	6	8.67	2.50
Total	20	99.41	1.02	15	99.98	1.02	23	100.1	1.1	16	99.22	0.88	6	98.38	0.85
Cr (ppm)	20	12.5	4.3	15	10.7	2.5	23	9.6	1.4	16	339.4	27.7	6	45.0	38.2
Ni	13	4.7	2.3	11	3.3	1.3	16	1.3	1.3	5	91.3	10.7	2	15.1	11.5
Co	13	4.6	1.8	11	2.7	0.9	16	4.9	8.2	5	42.1	2.4	2	28.3	4.0
Sc	13	11.4	1.4	11	5.3	1.5	16	4.2	0.8	5	29.7	1.3	2	31.6	1.7
V	20	29.1	4.8	15	17.9	4.5	23	12.3	5.2	16	219.8	14.4	6	307.7	19.2
Cu	13	19.6	25.7	11	7.4	4.0	16	51.5	82.1	5	42.0	27.5	2	10.1	10.1
Pb	13	25.8	45.8	11	47.1	29.8	16	145.5	226.2	5	120.9	209.9	2	10.2	3.9
Zn	13	175.9	200.6	11	196.1	277.2	16	420.3	443.1	5	190.9	137.6	2	185.8	68.7
Bi	13	0.3	0.3	11	0.4	0.4	16	1.6	3.4	5	0.2	0.4	2	0.1	0.0
In	13	0.1	0.0	11	0.0	0.0	16	0.0	0.0	5	0.1	0.0	2	0.1	0.0
Sn	20	4.8	2.1	15	8.2	2.9	23	7.7	3.1	16	0.9	0.2	6	2.2	0.4
Ag	13	0.6	1.5	11	0.7	1.3	16	0.8	0.9	5	0.2	0.2	2	0.1	0.0
Rb	20	136.1	33.7	15	168.4	73.9	23	141.5	46.6	16	70.8	60.4	6	139.2	73.9
Cs	20	2.9	0.9	15	1.9	0.9	23	2.6	1.1	16	4.3	5.1	6	6.1	3.7
Ba	20	1516	623	15	3557	2594	23	1632	1889	16	1725	1717	6	1582	800
Sr	20	59.7	22.3	15	70.6	39.1	23	43.2	38.7	16	201.8	77.7	6	146.1	24.3
Ga	20	25.7	2.4	15	20.9	4.0	23	22.8	5.6	16	16.0	1.4	6	22.7	2.8
Ta	13	2.5	0.2	11	2.1	0.8	16	1.9	0.3	5	0.5	0.0	2	1.2	0.1
Nb	20	43.6	4.2	15	25.3	4.5	23	23.7	4.4	16	9.2	0.7	6	20.6	3.3
Hf	20	16.7	1.7	15	10.6	1.7	23	7.6	2.0	16	2.5	0.3	6	6.2	1.2
Zr	20	714.1	80.3	15	399.7	67.7	23	259.4	79.5	16	91.1	7.5	6	246.3	48.5
Y	20	53.9	6.1	15	40.4	6.5	23	41.5	12.3	16	20.3	2.0	6	32.5	3.7
Th	20	30.6	3.6	15	27.9	4.5	23	28.8	6.3	16	1.5	0.2	6	8.0	2.7
U	20	4.2	0.4	15	7.4	1.8	23	7.2	2.9	16	0.4	0.1	6	2.1	0.8
La	20	92.9	10.1	15	50.6	6.8	23	52.7	15.3	16	10.0	1.3	6	33.9	9.7
Ce	20	189.1	20.3	15	103.4	15.9	23	107.9	29.7	16	21.9	2.8	6	72.7	19.9
Pr	20	21.8	2.3	15	11.5	1.8	23	12.1	3.3	16	2.9	0.4	6	9.1	2.4
Nd	20	82.1	8.4	15	41.6	6.9	23	43.5	12.6	16	13.1	1.5	6	36.7	8.6
Sm	20	15.5	1.5	15	8.0	1.4	23	8.8	2.8	16	3.5	0.4	6	8.0	1.4
Eu	20	2.4	0.3	15	0.6	0.1	23	0.5	0.1	16	1.1	0.2	6	1.9	0.3
Gd	20	12.3	1.2	15	6.6	1.1	23	7.1	2.1	16	3.7	0.4	6	7.2	0.9
Tb	20	1.8	0.2	15	1.1	0.1	23	1.2	0.4	16	0.6	0.1	6	1.1	0.1
Dy	20	10.2	1.1	15	6.8	1.0	23	7.5	2.2	16	3.9	0.4	6	6.2	0.4
Ho	20	2.0	0.2	15	1.4	0.2	23	1.5	0.4	16	0.8	0.1	6	1.2	0.1
Er	20	5.6	0.6	15	4.2	0.6	23	4.3	1.2	16	2.3	0.3	6	3.5	0.3
Tm	20	0.8	0.1	15	0.6	0.1	23	0.6	0.2	16	0.3	0.0	6	0.5	0.0
Yb	20	5.1	0.5	15	4.1	0.6	23	4.0	0.9	16	2.1	0.2	6	3.2	0.1
Lu	20	0.8	0.1	15	0.6	0.1	23	0.6	0.1	16	0.3	0.0	6	0.5	0.0
Al_2O_3/Na_2O	20	69.3	66.1	15	49.4	43.6	23	98.0	89.8	16	41.0	68.3	6	82.6	64.9
Zr/TiO_2	20	0.1	0.0	15	0.1	0.0	23	0.1	0.0	16	0.0	0.0	6	0.0	0.0
Zr/Al_2O_3	20	48.0	3.7	15	29.3	1.1	23	19.1	2.9	16	6.1	0.5	6	18.4	1.6
Al_2O_3/TiO_2	20	25.7	2.2	15	42.1	1.4	23	57.5	9.2	16	12.2	0.9	6	5.6	0.2
Zr/Y	20	13.3	1.5	15	9.9	1.0	23	6.6	2.1	16	4.5	0.4	6	7.9	2.8
Zr/Nb	20	16.4	1.1	15	15.9	0.7	23	10.9	2.1	16	9.9	0.3	6	11.9	1.0
Zr/Ti	20	0.2	0.0	15	0.2	0.0	23	0.2	0.0	16	0.0	0.0	6	0.0	0.0
Nb/Y	20	0.8	0.1	15	0.6	0.1	23	0.6	0.1	16	0.5	0.0	6	0.7	0.2
La/Yb (cn)	20	12.4	1.6	15	8.3	0.8	23	8.9	2.5	16	3.2	0.2	6	7.0	2.0
Eu/Eu*	20	0.5	0.1	15	0.3	0.0	23	0.2	0.0	16	0.9	0.1	6	0.8	0.0
Nb/Nb*	20	0.3	0.0	15	0.2	0.0	23	0.2	0.1	16	0.8	0.1	6	0.5	0.2
Nb/Ta	13	17.6	0.8	11	12.7	2.1	16	12.0	0.9	5	16.3	0.6	2	15.9	0.6
Ti/Sc	13	308.0	19.7	11	394.5	72.3	16	371.6	57.4	5	231.6	2.6	2	403.9	2.9

Notes: Mean and 2σ Error Values for the 5 main identified groups of volcanic rocks at the ABM deposit; La/Yb ratio chondrite normalized (McDonough and Sun, 1995); Eu anomaly calculated $Eu/Eu^* = Eu_{PM}/(Gdpm \times Sm_{PM})0.5$, Nb anomaly calculated $Nb/Nb^* = Nb_{PM}/(Th_{PM} + La_{PM})$; PM = primitive mantle-normalized (McDonough and Sun, 1995)

Abbreviations: FA = Felsic A, FB = Felsic B, MA = Mafic A, MB = Mafic B

and underlying FB rocks. The laterally most extensive argillite lens separates the two lithofacies domains, where volcaniclastic rocks are more abundant in Sequence 3, in contrast with voluminous subvolcanic and volcanic rocks in Sequence 2. No crosscutting volcanic or subvolcanic units with the FA signature are present in Sequence 2.

Sequence 3: The felsic volcanic and volcaniclastic rocks that are a part of Sequence 3 consistently have group FA signatures. The volcanic and volcaniclastic rocks likely have a common magma source. Thin mafic sills of the MB group intrude FA felsic volcanic and volcaniclastic rocks. The MB group of mafic rocks has similar signatures to the mafic rocks of the Wind Lake formation (Piercey et al., 2002b; Manor and Piercey, 2019) that occur in the immediate hanging wall of Sequence 3. Thus, the MB sills in Sequence 3 are likely coeval with the mafic rocks of the Wind Lake formation and likely acted as feeders.

Krakatoa zone: The Krakatoa zone exhibits the same distribution of geochemical groups as the ABM zone (Fig. 12). In Sequence 2, the FB1 group felsic sills are surrounded by group MA mafic sills; felsic rocks in the hanging wall and footwall of the thickest mafic sill have group FB2 signatures. Within Sequence 3, most of the felsic rocks are group FA, except for minor felsic lava flows approximately 50 m below the Kudz Ze Kayah-Wind Lake formation contact that have FB signatures.

Barium distribution

The majority of presented Ba values (N = 8989) are sourced from the assay database of BMC Minerals Ltd. The quality assurance and quality control procedures for assays are presented in van Olden et al. (2020). The Numeric Models tool in Leapfrog 3D was used to construct isosurfaces of Ba distribution (Figs. 4, 11, and 12). The linear radial basis function (RBF) interpolation was chosen to mitigate the irregular distribution of the almost 9,000 Ba datapoints. The linear RBF interpolant was run with a sill value of 5000, base range of 50, nugget of 0, and accuracy of 20. The trend was set to the local stratigraphy (dip 30° with dip azimuth of 20° and pitch of 115°) and the ellipsoid ratios were set to 3:3:1. The threshold value

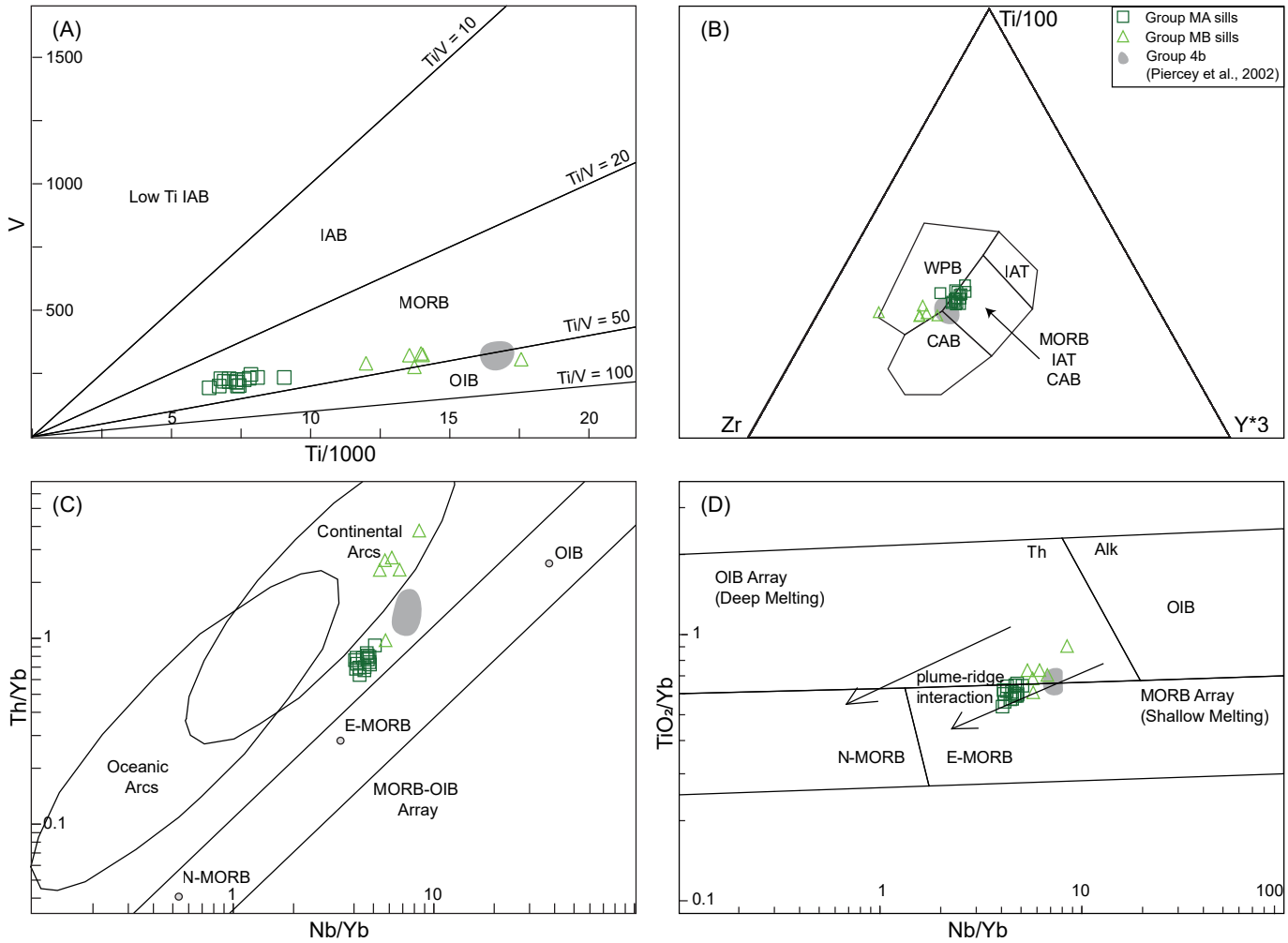

Figure 10. Trace element discrimination plots for mafic rocks in the ABM deposit. (A) Ti*1000 vs. V (Shervais, 1982). (B) Zr - Y*3 - Ti/100 (Pearce, 1996). (C) Nb/Yb vs. TiO_2/Yb (Pearce, 2008). (D) Nb/Yb vs. TiO_2/Yb (Pearce, 2008). Symbols same as in Figure 8. Gray shaded areas represent group 4b of the Wind Lake formation described by Piercey et al. (2002b). Abbreviations: CAB = calc-alkaline basalts, E-MORB = enriched mid-ocean ridge basalt, IAB = island arc basalts, IAT = island arc tholeiites, MA = Mafic A, MB = Mafic B, OIB = ocean island basalts, WPB = within plate basalts.

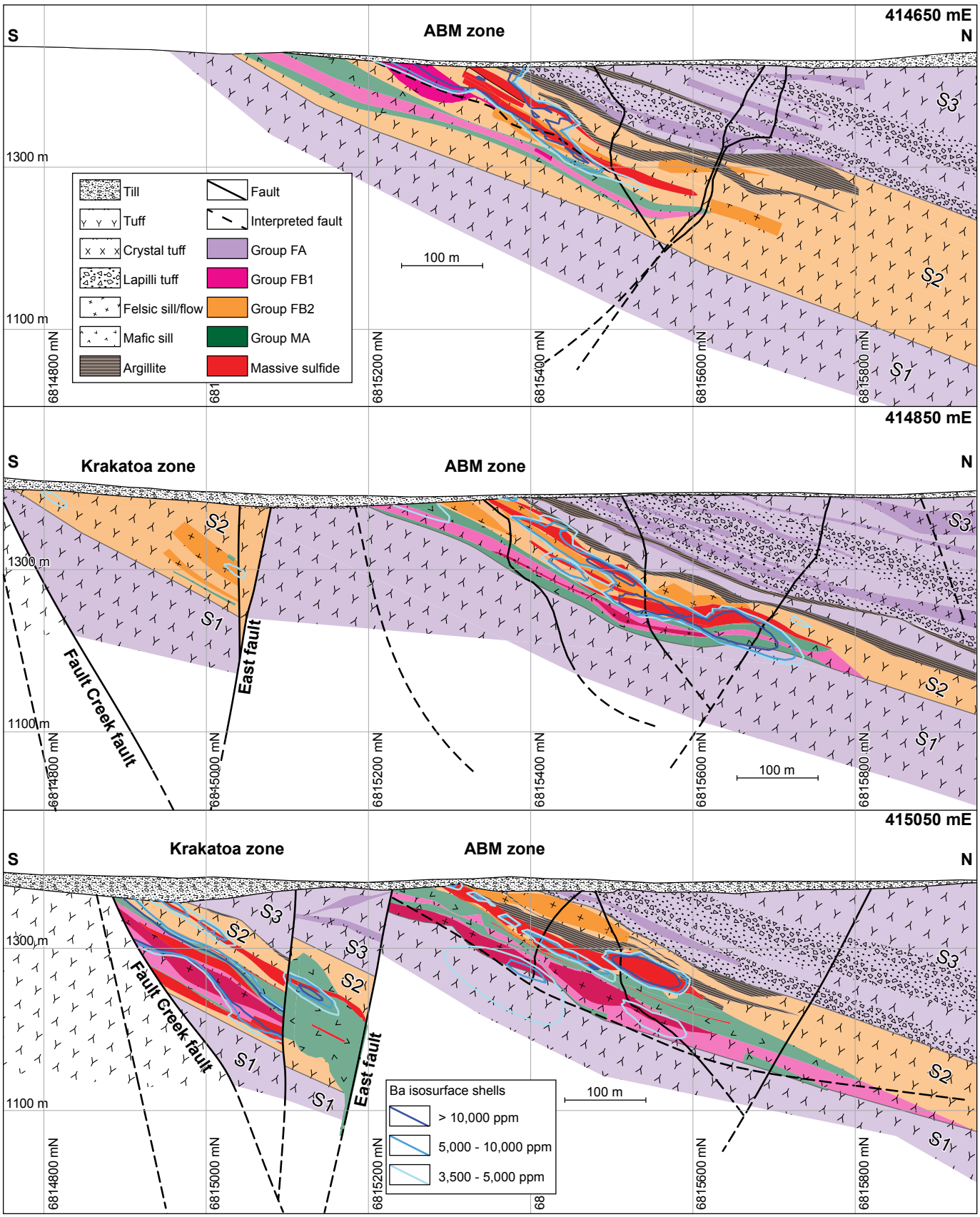

Fig. 11. Cross sections through the ABM zone of the ABM deposit; cross sections are looking west. Positions of section lines shown in Figure 3. Abbreviations: FA = Felsic A, FB = Felsic B, and MA = Mafic A, S1 = Sequence 1, S2 = Sequence 2, S3 = Sequence 3.

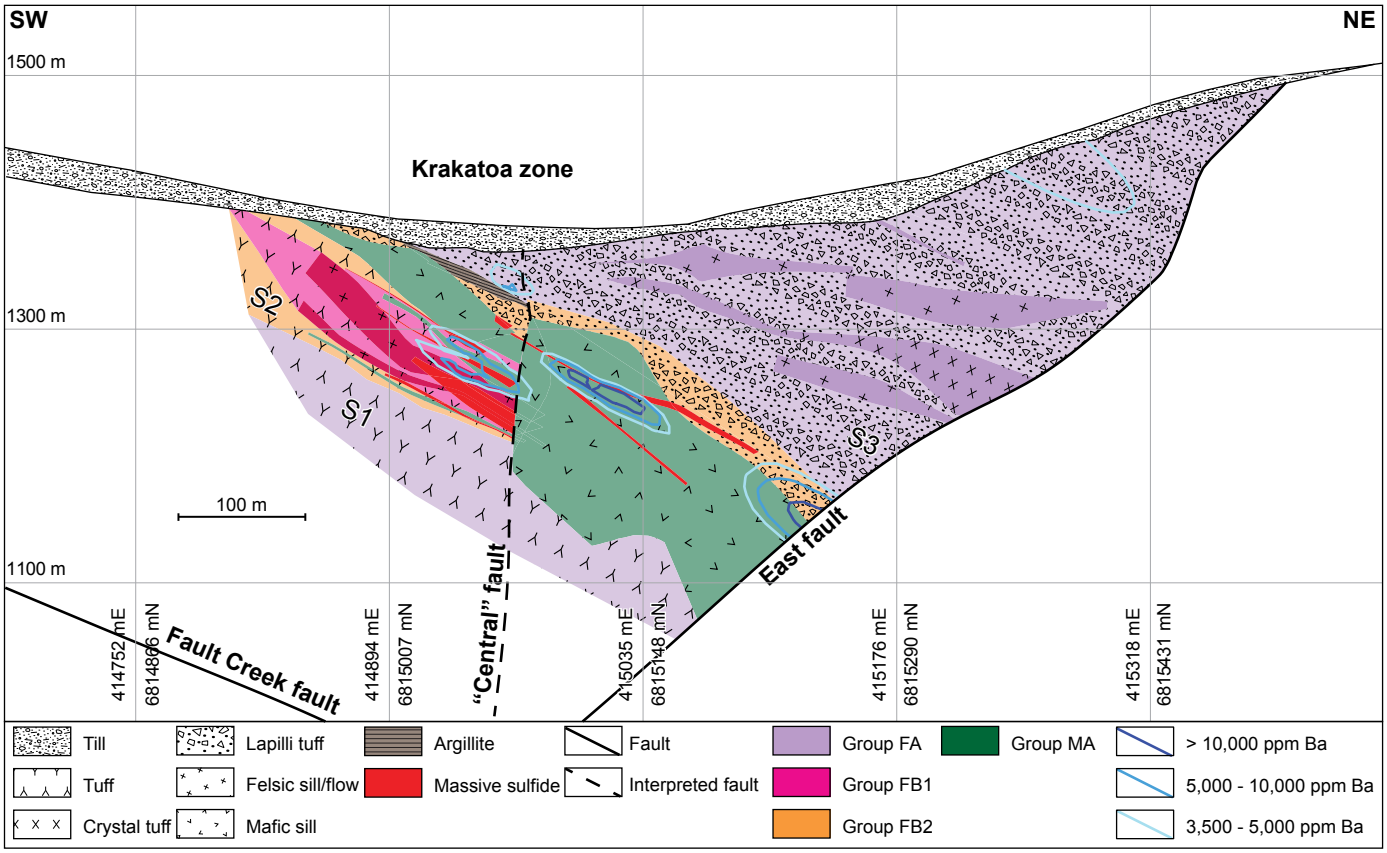

Fig. 12. Cross section through the Krakatoa zone of the ABM deposit; cross section is looking northwest. Position of section line shown in Figure 3. Abbreviations: FA = Felsic A, FB = Felsic B, and MA = Mafic A, S1 = Sequence 1, S2 = Sequence 2, S3 = Sequence 3.

for Ba at the deposit was chosen at 3,500 ppm using methods outlined in Reimann et al. (2005). Values above the threshold are considered anomalous and reflect Ba enrichment, as felsic volcanic rocks not associated with VMS deposits commonly show Ba values around 1229 ± 781 ppm (highest average value for felsic volcanic rocks reported for the Kudz Ze Kayah formation; Piercey et al., 2001). Anomalous Ba values occur in the vicinity of the massive sulfide mineralization at the ABM deposit and are associated with strongly altered rocks. Barite is a common gangue mineral at the ABM deposit; it is associated with the pyrite-sphalerite-galena assemblage (Fig. 7D), and minor Ba-rich feldspar and Ba-rich mica occur within the massive sulfide mineralization and the enveloping alteration zones (van Olden et al., 2020).

Discussion

Ancient VMS and modern sea-floor massive sulfide (SMS) deposits occur in numerous tectonic settings but are all associated with extensional tectonic environments (Lentz, 1998; Franklin et al., 2005; Piercey, 2011). Extensional back-arc basins that host VMS deposits have distinguishing features in the rock record, including distinctive lithofacies associations (Cas and Wright, 1987; McPhie et al., 1993), specific geochemical signatures (Lesher et al., 1986; Hart et al., 2004; Piercey, 2011), structures accommodating extension (Gibson et al., 1999; Mumin et al., 2007), and alteration haloes and zones around deposits (Gemmell and Large, 1992; Large et al., 2001a). Recognizing these features is important for regional and local exploration targeting in known (and unknown) VMS districts, and for decoding the conditions and circumstances that governed the formation of VMS mineralization. In newly identified prospective districts, identifying key features of prospective horizons enables more efficient assessment of the stratigraphy and helps focus more targeted exploration efforts. These themes will be further examined below.

Basin reconstruction

In subduction environments, back-arc basins are generated due to extension of the upper plate, where crustal thinning is accommodated by synvolcanic and/or synsedimentary normal faulting (Uyeda and Kanamori, 1979; Sdrolias and Müller, 2006). In modern rift settings, extension can be accommodated by pull-apart basins, a series of half-graben subbasins with horsetail mesh structures or similar structural arrangements (Parson and Wright, 1996; Sibson, 2000, and references therein), and similar configurations can be expected in ancient back-arc basins. In such ancient environments, VMS deposits are commonly associated with volcanic centers in low order basins (Allen et al., 2002). Synvolcanic faults in these basins typically control the rates of subsidence and the seafloor topography and can also act as conduits for magmas and hydrothermal fluids (Gibson et al., 1999). Movement on normal synvolcanic faults can be reversed during basin inversion, which allows for some of these deeply penetrating structures

to be preserved, albeit as thrust or transform faults (e.g., East fault; Fig. 3; Nelson, 1997; Lafrance et al., 2020). Lithofacies associations can identify important features of the basin, such as proximity to a volcanic center, rapid burial rates, periods of volcanic quiescence, or structural features. The host rocks of the ABM deposit display features typical for an active and proximal volcanic center in a lower-order subsidence basin; several features also point to the presence of active synvolcanic faults. Chemostratigraphy and lithofacies analysis further constrain the relative timing of the different processes that contributed to the formation of the ABM deposit.

Features within the Kudz Ze Kayah formation indicate that the rocks were deposited in a submarine basin at depths between 500 and 2,000 m below sea level, like modern VMS analogues in back-arc settings (Monecke et al., 2014). These features include lack of diagnostic sedimentary textures, such as evidence for storm beds with hummocky cross-stratification suggesting deposition at depths below the storm base (>500 m; Gibson et al., 1999). Further, there is no evidence of hydrothermal fluid boiling or phase separation within the mineralization, which suggests a water depth of at least 500 to 1,000 m (Monecke et al., 2014). The presence of primary Cu-rich mineralization indicates water depths of at least 1,500 m, as fluids that carried Cu would require temperatures of at least 300°C (Franklin et al., 2005; Hannington et al., 2005) and these fluids are only stable at water depths >1,500 m (Bischoff and Rosenbauer, 1987; Hannington et al., 2005). So, while the water depth is often difficult to interpret in ancient basins, a rough estimate is beneficial for understanding of the volcanic and sedimentary processes active in the basin, and our arguments suggest formation at least 1,500 m below sea level (or deeper).

A common feature of VMS deposits, regardless of water depth, is the temporal and spatial association of VMS mineralization with active volcanic centers, commonly marked by the occurrence of felsic lava flows and/or domes reflecting proximity to volcanic vents and synvolcanic structures that facilitated hydrothermal venting during periods of volcanic quiescence (McPhie et al., 1993; Gibson et al., 1999; Franklin et al., 2005). The occurrence of abundant primary crystal-rich tuff units in the stratigraphy at the ABM deposit, and their chemical similarities and interlayering with coeval coherent rocks (Figs. 4, 11, and 12), is consistent with emplacement proximal to a volcanic center (e.g., Cas and Wright, 1987). The coeval emplacement of flows and sills with the volcaniclastic rocks is also indicative of a relatively dynamic volcanic environment of magma/volcaniclastic emplacement (e.g., Head and Wilson, 2003). Further, the abundance of coherent volcanic rocks interlayered with crystal-rich volcaniclastic rocks proximal to the ABM deposit suggests that the association of these facies with mineralization at ABM is not coincidental and that the deposit area was proximal to a volcanic center during the deposition of all three sequences of the upper Kudz Ze Kayah formation. The relative abundance of coherent volcanic rocks, and relatively minor volcaniclastic rocks, in the Krakatoa zone compared to the ABM zone suggests that the Krakatoa zone was even closer to a potential volcanic center than the ABM zone.

Another feature of back-arc basins that is also essential for the existence of volcanic centers is the presence of synvolcanic faults, as normal movement on the faults accommodates crustal extension, deepens the basins, and can cause significant changes in topography within lower-order basins (Halbach et al., 1993; Kerr and Gibson, 1993). Synvolcanic faults are commonly responsible for abrupt changes in thickness or terminations of units in their footwall, whereas units in their hanging wall are commonly not affected (Gibson et al., 1999), and in some cases, synvolcanic faulting segments the basin topography, which results in features such as drape folds (Mumin et al., 2007). Stratigraphic reconstruction of the upper Kudz Ze Kayah formation has identified numerous units of volcanic, volcaniclastic, and sedimentary rocks that can be traced up to 1.4 km along strike through the footprint of the ABM zone. The thickness of the identified volcaniclastic and sedimentary units varies significantly in as little as 50 m strike distance (Figs. 4, 11). We interpret that the changes in thickness were caused by deposition in a fault-bound basin, where synvolcanic faults created abrupt changes in the topography of the sea floor that resulted in thinning of the units in the footwall of the fault and thickening and accumulation of volcaniclastic and sedimentary material in the hanging wall of the fault. The changes in thickness are most easily observed in argillite lenses, which are locally strongly reminiscent of drape-folds (Figs. 4, 11; Mumin et al., 2007), typical of a basin with active synvolcanic faults. Minor later modification of the units by the active synvolcanic faults was also likely. The interpreted fault planes of the synvolcanic faults are irregular, which is typical for a heterogenous environment such as a back-arc extensional basin (Rissmann et al., 2011). It is notable that the effects of normal movement along the synvolcanic faults can be observed up to the Kudz Ze Kayah-Wind Lake formation contact, which suggests that the synvolcanic faults were active throughout the deposition of the entire Kudz Ze Kayah formation.

Synvolcanic faults are also known to act as magma conduits and to control emplacement of sills, dikes, felsic flows, domes, or cryptodomes (Sibuet et al., 1998; Gibson et al., 1999; Winter et al., 2004; Franklin et al., 2005), and the alignment of such rocks can also be used for reconstructing synvolcanic faults. In the ABM zone, felsic sills and flows thicken in proximity to certain faults, but thin out laterally or terminate in proximity to other faults (Figs. 4, 11), which suggests that the interpreted synvolcanic faults acted intermittently as conduits for the ascending felsic magmas. The mafic subvolcanic sills also show systematic changes in unit thickness and alteration, indicating their emplacement was also controlled by synvolcanic faulting (Figs. 4, 11). Further, the occurrence of volcanic units with varying signatures (FA, FB, MA) proximal to one another near the same interpreted synvolcanic faults also implies that these faults acted as conduits for magmas throughout the duration of volcanic activity in the basin.

Synvolcanic faults in the ABM zone occur in two dip directions (Fig. 3): 1) 075° to 105° with dips between 60° and 85°, and 2) 150° to 180°, with dips 75° to subvertical. The faults are interpreted to be splays of and subordinate to the regional East fault, which was likely one of the major faults controlling subsidence in the basin. The fault arrangement in the ABM zone (Fig. 4) is reminiscent of either a set of listric faults subordinate to the East fault, a pull-apart basin, or a series of half-graben subbasins with horsetail mesh structures; any of

these configurations can occur in a modern subsiding basin (Parson and Wright, 1996; Wright et al., 1996). The orientation of the above-described drape folds, the thickening of the volcaniclastic and sedimentary units toward the southeast and the East fault, and the general thickening of Sequence 2 toward the East fault implies the that the basin hosting the ABM deposit was deepening in that direction (i.e., deepening toward the southeast).

Precipitation mechanisms for mineralization

Ore and gangue minerals in VMS systems precipitate due to fluid mixing between hot, acidic, metal-rich hydrothermal fluids (T = 200°–350°C, pH ~2–5; Hannington et al., 2005 and references therein) and cold seawater (~ 2°C; Haymon, 1983). Up to 90% of the metals within the hydrothermal fluids vent into the ocean and are lost if the mixing occurs at the sea floor (Converse et al., 1984). However, if the hydrothermal fluids are introduced to water-saturated facies beneath the sea floor, fluid mixing, sulfide precipitation, and zone refining can be more efficient at forming massive sulfide deposits (Doyle and Allen, 2003; Piercey, 2015). Replacement-style VMS deposits can form anywhere between 0 and 10 m depth down to 200 mbsf, where volcaniclastic facies remain porous and permeable (Doyle and Allen, 2003) and lateral fluid flow is possible (Piercey, 2015); they also require the presence of nonpermeable to semipermeable units (sills, lava flows, argillites) within the stratigraphy that act as barriers for fluid flow, and rapid burial rates for most effective sulfide precipitation and preservation (Doyle and Allen, 2003). At the ABM deposit, felsic volcaniclastic rocks comprise a significant portion of the deposit-hosting stratigraphy. Felsic lapilli tuffs in the upper Kudz Ze Kayah formation display features typical for subaqueous mass flows or eruption-fed density currents (Cas and Wright, 1987; McPhie et al., 1993; White, 2000). The lapilli tuffs are generally massive, unsorted to poorly sorted (Fig. 6F-G) with singular units that can be spatially extensive (>0.5 km^2) compared to the felsic coherent units (maximum of 0.12 km^2 in ABM), and over 50 m thick, which implies rapid accumulation and burial (McPhie et al., 1993; White, 2000). The thickest units occur in Sequence 3, but lapilli tuffs occur throughout the upper Kudz Ze Kayah formation, indicating that the style of volcanism remained relatively unchanged throughout the deposition of the upper Kudz Ze Kayah formation. Interpreted porous and permeable lithofacies (e.g., lapilli tuffs, crystal-rich tuffs, and brecciated contacts of sills and flows) that were likely saturated with seawater in the shallow subsurface were interbedded with relatively impermeable lithofacies (e.g., coherent volcanic facies and possibly lithified mudstones/argillites) that likely acted as barriers to fluid flow. Moreover, it is possible that coherent portions of volcanic units and possibly semipermeable argillite lenses acted as aquitards that prevented upward flow of fluids along the synvolcanic faults (e.g., Mumin et al., 2007), diverting hydrothermal fluids laterally into the water-saturated, unconsolidated volcaniclastic or brecciated rocks. This diversion would have resulted in fluid mixing between hot hydrothermal fluids and infiltrated seawater in the volcaniclastic rocks and formation of replacement fronts comprising sulfide mineralization and irregular alteration zones; these features are observed in drill core emanating outwards from inferred synvolcanic faults (Figs. 4, 11). The lateral flow of the hydrothermal fluids within porous and water-saturated units also resulted in the formation of laterally continuous massive sulfide lenses that parallel stratigraphy. Thus, this juxtaposition of lithofacies with varying porosity and permeability proximal to synvolcanic faults controlled the hydrothermal fluid flow, mineralization, and distribution of the alteration within the upper Kudz Ze Kayah formation.

Subseafloor replacement also creates distinctive hydrothermal alteration patterns. In the ABM deposit, replacement-style mineralization is closely associated with pervasive white mica alteration; however, unlike in exhalative mineralization, pervasive white mica alteration occurs in both the hanging wall and footwall to mineralization. This can be explained in two different ways, both of which are consistent with subseafloor replacement. One possible explanation of this is that the hanging wall to the mineralization was present during hydrothermal activity and sulfide formation, and that the mineralized interval was within 200 m of the sea floor and not diagenetically sealed, since hydrothermal alteration is documented all the way to the contact with the Wind Lake formation (Doyle and Allen, 2003). The alternative explanation is that the extended hanging wall to the mineralization (Sequence 3) was absent during the main mineralizing event, but lower-temperature hydrothermal activity continued intermittently during its later deposition. The absence of significant mineralization in Sequence 3 rocks is consistent with the second possibility and indicates that the hydrothermal activity continued throughout the basin evolution, albeit at temperatures lower than those necessary to precipitate mineralization.

The alteration and replacement fronts outlined above are also reflected in the distribution of Ba in the ABM deposit. Barium is a common component of hydrothermal fluids and precipitates as Ba minerals due to mixing of the hydrothermal fluids with seawater (Von Damm, 1990; Averyt and Paytan, 2003). Barium-rich minerals such as barite, Ba-rich white mica (Large et al., 2001a; Soltani Dehnavi et al., 2019), and Ba-rich feldspar are commonly associated with massive sulfide mineralization (Lydon, 1984; Franklin et al., 2005). At the ABM deposit, the highest Ba values occur nearest to the 075°-105° set of synvolcanic faults, suggesting that the hydrothermal fluids upwelled along these faults. The decrease of Ba values along and within sills and flows indicates these units had low permeability and acted as local fluid barriers (Fig. 4). In addition, Ba distribution (Figs. 4, 11) suggests that the immediate hanging wall of the massive sulfide mineralization, comprising the proximal overlying argillite lenses and the volcaniclastic rocks in between, acted as a semipermeable barrier/aquitard for upwelling hydrothermal fluids and were consequently altered by Ba-rich hydrothermal fluids during the mineralization stage. Moreover, the lateral distribution of Ba into units away from synvolcanic faults is also supportive of the Ba- and metal-rich fluids having infiltrated laterally away from synvolcanic structures into the unconsolidated volcaniclastic rocks. In the Krakatoa zone, it appears that the mafic sills acted as a partial aquitard for the hydrothermal fluids, as anomalous Ba values occur predominantly in the footwall of the mafic sills or are associated with the mineralized lenses (Fig. 12).

We suggest that the distribution of anomalous Ba values is not caused by a later hydrothermal or metamorphic overprint

but represents the original fluid pathways and extent of the hydrothermal system that formed the massive sulfide mineralization and associated alteration zones. We base this on the close association of Ba-rich minerals and anomalous Ba values with massive sulfide mineralization (Figs. 4, 11, and 12) and the presence of hanging-wall alteration that exhibits minor Ba enrichment. The presence of argillite in the hanging wall, together with the Ba distribution, suggest that mineralization coincides with a break in volcanism, which is also reflected by the change in chemistry from FB rocks in Sequence 2 to FA rocks in Sequence 3, indicating that mineralization formed during the waning stages of the FB cycle or during the commencement of the second FA cycle.

The period of volcanic inactivity between Sequence 2 and Sequence 3 was likely at minimum 75 k.y., based on estimates of settling rates of argillites from the Middle Devonian (e.g., Goodfellow and Turner, 1989). Estimates calculated from the maximum thickness (adjusted for the drill hole dip) of the thickest argillite lens (9.85 m, not corrected for thickness changes due to diagenesis) and average shale deposition rates (13 cm/1,000 y) from a similar sediment-hosted deposit type (e.g., Goodfellow and Turner, 1989) yield a minimum age of 75,000 years. These rates are similar to the timeframes of modern SMS deposits (Jamieson et al., 2014) and those recently calculated for deposits in the Finlayson Lake district (e.g., Manor et al., in press).

The ABM deposit has highly anomalous Zn grades (6.6 wt %), and above average tonnage for VMS deposits globally (19.1 Mt; Piercey et al., 2015). We suggest that the grade and tonnage in the ABM deposit was partly controlled by the basin architecture and magmatic activity. In particular, the permeability contrasts between various lithofacies coupled with fluid flow controlled by synvolcanic faults allowed for replacement-style mineralization, which we suggest enhanced both the amount of metal precipitated from the hydrothermal fluids and increased the efficiency of zone refining, which led to increases of the Zn grade (e.g., Piercey, 2015). These results demonstrate the critical importance of understanding basin architecture and sulfide emplacement processes and its potential influence on grade and tonnage in ancient VMS deposits. By understanding such features and developing criteria for recognizing them, it may be possible to determine similar geologic environments globally that have similar potential for high value deposits

Relationship between ABM and Krakatoa zones

While the distribution of lithogeochemical groups and lithofacies is similar in both zones, the transition between the ABM and Krakatoa zones is unclear due to the dextral-oblique offset on the East fault (Fig. 3). For example, the mineralization in the eastern part of the ABM zone occurs as a single massive sulfide lens with argillite and tuff in its hanging wall that terminates on the East fault. The corresponding mineralization in the Krakatoa zone, however, comprises several massive sulfide lenses located on the upper and lower contacts and within the MA mafic sill. This suggests that the hydrothermal system in the two zones was likely active during a similar time period, that is, after the emplacement of MA sills and the emplacement and deposition of Sequence 1 and 2 felsic rocks, but it is unclear whether the alteration and mineralization in the two zones are part of the same hydrothermal system, with the transition between the ABM and Krakatoa portions eroded from the Krakatoa block due to the offset and rotation of the block, or the two hydrothermal systems formed in separate lower-order basins on each side of the East fault and tapped the same source of hydrothermal fluids, likely along the East fault itself. Further studies of the hydrothermal alteration and ore assemblages in both zones are necessary to determine whether the two zones are part of one hydrothermal system or if they represent two distinct deposits in separate lower-order basins.

Petrogenesis of felsic and mafic rocks

Results of this study echo previous regional-scale research (Piercey et al., 2001, 2002b, 2003; Murphy et al., 2006; Manor and Piercey, 2019) but provide further details on the petrogenesis of the felsic and mafic volcanic rocks that host the ABM deposit. Piercey et al. (2001, 2003) noted anomalously high contents of high field strength elements (HFSEs) and rare earth elements (REEs) in the felsic rocks of the Kudz Ze Kayah formation. Our study further refines the lithostratigraphy and has identified two distinct lithogeochemical groups of felsic rocks within the upper Kudz Ze Kayah formation: 1) the FA group, which has relatively high Zr values compared to felsic rocks hosting similar felsic-hosted VMS deposits in the geologic record (e.g., Lentz, 1998), and 2) the FB group, which has lower HFSE-REE contents compared to the FA group. Both groups have calc-alkaline affinities and plot as within-plate and A-type felsic rocks (Fig. 8; Pearce et al., 1984; Whalen et al., 1987; Ross and Bédard, 2009), and their PM-normalized patterns are alike (Fig. 9). Even though chondrite-normalized plots show distinct differences in the intensity of the negative Eu anomaly, the similarities between the two lithogeochemical groups and their close spatial association suggest that the two groups have likely melted a common source, most likely continental crust (Piercey et al., 2001, 2003) that was partially melted at relatively low pressures and high temperatures (e.g., Hart et al., 2004 and references therein). However, the differences in absolute Zr and REE contents, Eu-anomalies, and some immobile element ratios (i.e., Zr/Al_2O_3, Al_2O_3/TiO_2, Zr/Y, Ti/Sc) indicate that the two groups formed at differing conditions, likely forming from melts that were generated at varying temperatures (Piercey et al., 2003). The magmas that formed the FA group felsic rocks likely formed at higher temperatures than the rocks of the FB group, as melting temperatures can control the HFSE-REE budget of continental crust-derived melts (Harrison and Watson, 1983; Watson and Harrison, 1983; Bea, 1996; Lentz, 1998; Piercey et al., 2003, 2008; Hart et al., 2004). Both felsic groups have LREE enrichment and display negative Nb and Ti anomalies in PM-normalized plots, features similar to felsic magmas generated from the remelting of continental arc crust and/or continental crust in general (Morris et al., 2000), which fits with the general continental back-arc setting for these rocks (Piercey et al., 2001). Past studies also suggested mantle-crustal mixing due to juvenile basaltic underplating (Piercey et al., 2001, 2008), which would impart some mantle-like trace element signatures onto the felsic rocks. One of these proxies that identifies such inputs is the Nb/Ta ratio that is commonly used to distinguish between mantle (Nb/Ta ~17)

and upper continental crustal sources (Nb/Ta ~12; Green, 1995; Barth et al., 2000; McLennan et al., 2003). Group FA rocks show higher average values of the Nb/Ta than rocks of group FB (FA ~17.8 vs. FB ~12.0), indicative of a higher juvenile mantle input into the FA group magmas, a consequence of upwelling of basaltic magmas and crustal underplating in an extending back-arc basin (Piercey et al., 2008; Piercey, 2011). Another possible explanation for the higher Nb/Ta values could be the fractionation of a Ti phase during the ascent of the magma, such as titanite and rutile, that favors Ta over Nb (Green and Pearson, 1987; Green, 1995). This is unlikely, however, as the FA group has higher Ti values than the FB group, and Ti minerals such as rutile were observed in thin section in both felsic rock groups. Comparing the Ti/Sc values for the two groups, the FB group has higher average values (FA ~308 vs. FB ~380), which are still lower than typical upper crust values (~445; Wedepohl, 1995) and indicative of a lesser input from juvenile sources to the FB group than to the FA group (Wedepohl, 1995; McLennan et al., 2003; Piercey et al., 2008). The presented trace element signatures (Nb/Ta, Ti/Sc) indicate that both groups display evidence of mixing with juvenile basaltic material, but the FA group rocks have a greater juvenile component compared to the FB group rocks.

The spatial association of the FB1 felsic rocks with the MA mafic sills confirms bimodal magmatism in the upper Kudz Ze Kayah formation. The FB1 felsic sills and tuffs were emplaced and deposited early in the evolution of the ABM basin, given that the MA mafic sills intruded along the contacts of the FB1 felsic sills, and both are hydrothermally altered (Fig. 13A, B). The felsic rocks of the upper Kudz Ze Kayah formation (FA and FB groups) are interpreted to be products of crustal melting due to basaltic underplating, and it is likely that the associated mafic rocks formed by modification of leaked and upwelling basaltic magmas along synvolcanic conduits. These MA group mafic rocks have transitional to calc-alkaline signatures (Fig. 8) and plot in to the MORB, E-MORB and WPB fields (Fig. 10). These signatures are common for mafic rocks within evolved continental to back-arc environments (Piercey, 2011) and point to an enriched mantle source and/or a source/magmas that were contaminated by continental crust (Pearce, 1996). Relative to the overlying Wind Lake formation mafic rocks, the MA mafic rocks have lower degrees of crustal contamination, as demonstrated by the Th/Yb-Nb/Yb and Th/Nb-Zr diagrams (Fig. 10C), possibly due to shorter residence times in the crust and/or due to faster rates of magma ascent (Gamble et al., 1995; Piercey et al., 2002a), while having a similar mantle source as the Wind Lake formation mafic rocks. This argument is supported by the similar Nb/Ta for both groups, ~16, indicating a mantle of either lithospheric or asthenospheric origin (Piercey et al., 2001, 2008). Although the mafic sills with MA signatures occur throughout Sequence 2 in the deposit area, their volume is relatively minor compared to the Wind Lake formation mafic rocks regionally. The MB mafic rocks, occurring as relatively thin mafic sills intruding mostly Sequence 3 rocks, have geochemical signatures similar to those of the mafic tuffs in the Wind Lake formation, specifically to the "4b" groups of Piercey et al. (2002b; Fig. 10). The occurrence of mafic sills with MB signatures at the top of Sequence 3 (Fig. 4) suggests that the mafic tuffs at the base of the Wind Lake and the MB mafic sills have a common source and formed roughly at a similar time, after the deposition of Sequence 3 (Fig. 13E).

Most known VMS deposits are interpreted to be associated with hot, shallow synvolcanic intrusions that are comagmatic with rhyolitic volcanism and they are interpreted to have acted as heat sources for the developing VMS hydrothermal systems (Galley, 2003; Franklin et al., 2005). In some cases, spatially associated subvolcanic intrusions postdate the VMS mineralization (Galley, 2003; Barrote et al., 2020) and are viewed as indicators of elevated heat gradients in the rift environment, due to their crystallization ages being younger than the VMS deposits, rather than the immediate drivers of VMS hydrothermal circulation (Hart et al., 2004; Piercey, 2011). Volcanic rocks in the Kudz Ze Kayah formation have similar compositions to the Grass Lakes Plutonic Suite intrusive rocks (Piercey et al., 2003; Murphy et al., 2006; Manor and Piercey, 2019), and the latter have been hypothesized as the heat source for the ABM hydrothermal system (Piercey et al., 2003). However, recent U-Pb geochronology in the district has shown that the plutonic suite postdates the deposition of the upper Kudz Ze Kayah formation by ~900 k.y. (Manor et al., in press); thus, these granitoids did not directly contribute to the heat flow regime that generated the ABM deposit, but they are likely the upper crustal manifestations of elevated geothermal gradients within a rift environment at a regional scale (e.g., Piercey et al., 2008; Piercey, 2011). The occurrence of multiple magmatic and volcanic events of varying composition ranging from mafic to felsic within the back-arc basin implies an enduring elevated heat gradient and, by extension, the likely presence of a heat corridor underlying the back-arc basin (e.g, Galley, 2003; Piercey, 2011).

This heat corridor also underwent heat gradient fluctuations as recorded by the litho- and chemo-stratigraphy of the upper Kudz Ze Kayah formation, which suggests potential heating and cooling cycles during its evolution. For example, the FA group REE-HFSE signatures show that they were likely generated at relatively higher temperatures relative to the FB group rocks, reflecting a high- to low-temperature cooling cycle (Piercey et al., 2001, 2003). It would be expected that the FA rocks should be associated with the VMS mineralization, given their high-temperature origin (Piercey et al., 2008; Piercey, 2011), yet the FA rocks are not directly associated with the massive sulfide mineralization, which is instead hosted by Sequence 2 rocks with FB signatures (Figs. 4, 11, and 12). Rather, the mineralization occurs in FB rocks in in the upper portions of Sequence 2 associated with argillite lenses at the transition from Sequence 2 to Sequence 3, indicating that the massive sulfide mineralization occurred during the waning stages of lower-temperature FB volcanic activity or during a period of volcanic quiescence before the restart of a second cycle of higher-temperature FA felsic volcanism (Fig. 13). During such a period of quiescence, the influx of FA magma into the chamber at depth could have acted as a heat source that sustained the mineralizing hydrothermal system (e.g., Cathles et al., 1997; Cathles, 2011). The duration of the period of volcanic inactivity at the transition from Sequence 2 to Sequence 3 was at minimum 75 k.y., as evidenced by the thickness of the argillite lenses, which fits within the timeframe of ~400 k.y. for the deposition of 250 m of stratigraphy in the upper part of the Kudz Ze Kayah formation (Manor et al., in press) and is typical

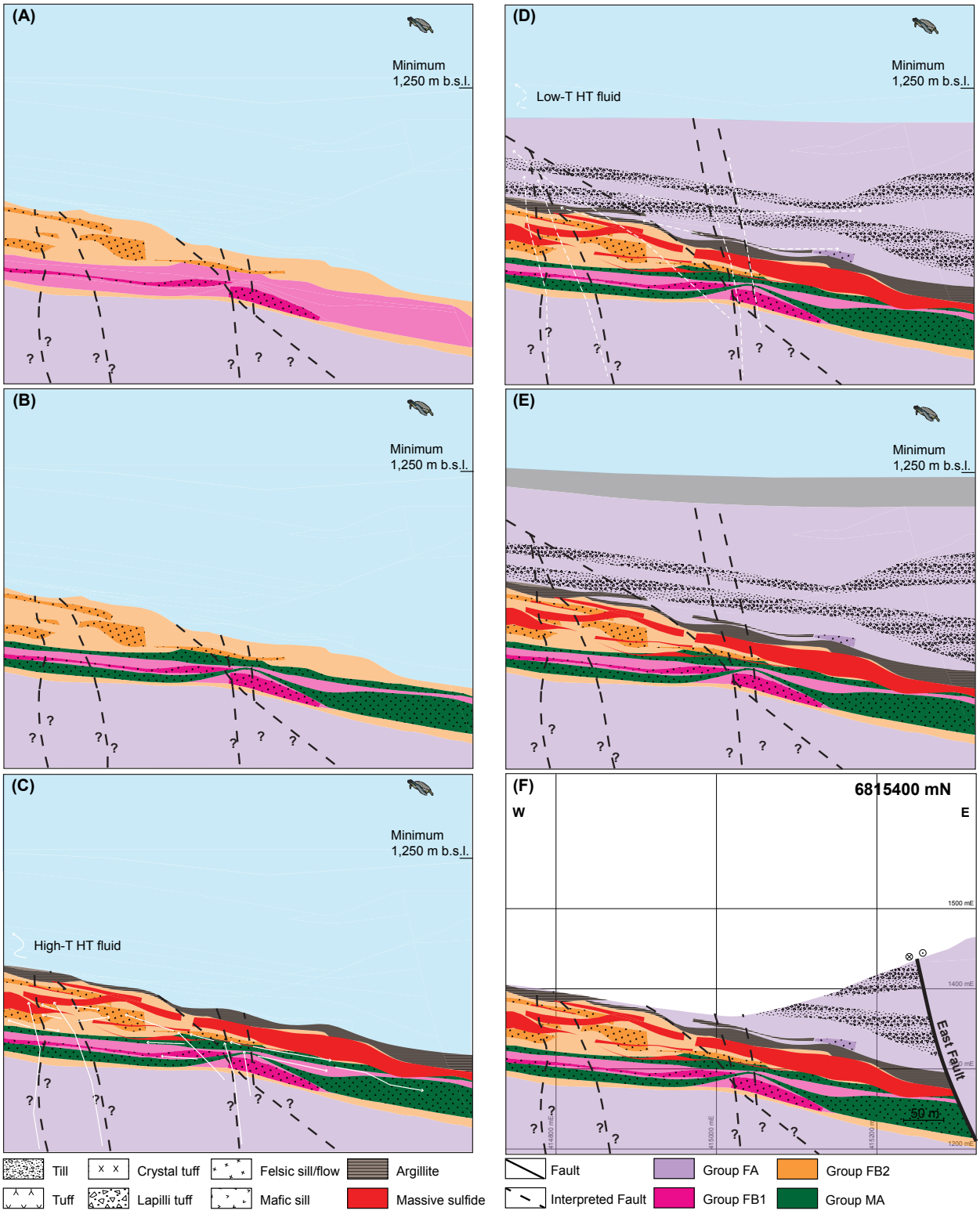

Fig. 13. Series of schematic diagrams of idealized stratigraphy of 6815400 mN long section though time showing the deposition of the upper Kudz Ze Kayah formation and the massive sulfide mineralization. (A) Deposition of Sequence 2 rocks with Felsic B (FB) signatures on top of Sequence 1 rocks with Felsic A (FA) signatures. In Sequence 2, rocks with FB2 signatures deposited first, followed by deposition of FB1 tuffs, emplacement of FB1 sills, and continued deposition of FB2 volcaniclastic rocks, flows, and sills. (B) Emplacement of Mafic A (MA) mafic sills along the contacts of pre-existing FB1 felsic sills. (C) Break in volcanism, argillite lenses deposited on top of Sequence 2, massive sulfide mineralization formed in the subsurface. (D) Deposition of Sequence 3 volcaniclastic and volcanic rocks with FA signatures. (E) Switch to mafic alkaline volcanism, deposition of Wind Lake formation rocks. (F) Current erosion level pictured without overlying till.

for the lifespan of VMS districts in the ancient record (<2 m.y.; Cathles et al., 1997; Franklin et al., 2005). The evidence for multiple heating cycles within the ABM stratigraphy implies that the mineralizing processes were associated with high-temperature magmatic pulses and input of juvenile material in the magma chamber, possibly during a high-temperature part of a magmatic cycle, similar to what is observed in continental arcs (De Silva et al., 2015). This suggests that the source for the heat that induced the hydrothermal system was prolonged and associated with a deep-seated magma chamber that elevated the crustal-level geothermal gradient, creating a thermal corridor that could sustain robust hydrothermal activity that led to VMS mineralization. Thus, in the Finlayson Lake district, shallow subvolcanic intrusions (and spatially associated mineralization) were a product of elevated geothermal gradient of the environment, but the subvolcanic intrusions themselves were not responsible for driving VMS hydrothermal circulation and deposit formation.

Conclusions

Reconstruction of the basin architecture of the Upper Devonian Kudz Ze Kayah formation shows that the rocks hosting the ABM VMS deposit were deposited in a back-arc basin at least 1,500 m deep with an active volcanic center and associated with synvolcanic faults. The identification of significant and systematic changes of the thickness of the sedimentary and volcaniclastic units, together with the distribution of coherent volcanic and subvolcanic rocks, allowed for the reconstruction of two sets of synvolcanic faults that were active during the deposition and emplacement of the lithostratigraphic units. Argillite lenses acted as semipermeable barriers at the top of the volcanosedimentary pile, trapping the hydrothermal fluids that ascended along synvolcanic faults and forcing them to permeate laterally into the subsurface, which likely resulted in more efficient sulfide precipitation and greater abundance of metals preserved and enhanced zone refining, and generated the elevated Zn tonnages and grades in the ABM deposit. The distribution of Ba can be used to map out areas with the most intense fluid flow, and in the ABM deposit, these coincide with synvolcanic faults, zones of pervasive alteration, and lenses of massive sulfide mineralization. The main argillite lens marks a period of volcanic quiescence that coincides with a change in the geochemistry of the footwall and hanging-wall felsic volcanic rocks and during which period the massive sulfide mineralization formed.

The reconstructed litho- and chemo-stratigraphy demonstrates that the ABM and Krakatoa zones were likely part of the same basin, but possibly in separate subbasins, with the Krakatoa zone likely closer to the volcanic center due to the higher relative abundance of coherent rocks. Mineralized lenses in both zones occur at roughly the same stratigraphic position and were either connected and part of the same hydrothermal system or they represent two separate systems but tap the same fluid source at depth.

Although they are not directly associated with the mineralization, FA group volcanic rocks at the ABM deposit serve as an important indicator of the elevated geothermal gradient in the basin, which is a key factor in the formation of VMS mineralization. High Zr values (>550 ppm), together with elevated HFSEs, REEs, and higher Nb/Ta ratios associated with the FA felsic volcanic rocks, reflect much higher temperatures and a higher degree of mixing of crustal melts with juvenile material compared to the FB felsic rocks. The cyclicity of the magma output represented by the systematic changes in geochemical signatures and the bimodal character of volcanism in the upper Kudz Ze Kayah formation suggest an elevated geothermal gradient within the back-arc basin due to the presence of a magmatically-driven thermal corridor underlying the basin. This elevated geothermal gradient was critical for driving hydrothermal circulation that formed the VMS mineralization at the ABM deposit.

The lithostratigraphic and geochemical features of the host rocks of the ABM deposit outlined in this study can be used as guidance for identifying prospective horizons and sequences in similar environments globally that formed within continental back-arc basins with associated bimodal volcanism.

Acknowledgments

This paper represents a part of the Ph.D. thesis by the first author. We would like to thank BMC Minerals Ltd. for their generous financial, field, and logistical support. Support for the project was provided by an NSERC Discovery Grant to Dr. Stephen Piercey, an NSERC Collaborative Research Development Grant – Project (CRDPJ) between Dr. Stephen Piercey and BMC Minerals Ltd., a Student Research Grant from the Society of Economic Geologists Canada Foundation, and funding from Memorial University of Newfoundland. We would like to thank Dr. Michelle DeWolfe, Dr. Steven Hollis, and Dr. Jonathan Cloutier for their detailed and constructive reviews of an earlier version of this manuscript that have greatly improved it. The senior author would like to thank Matthew Manor, Carly Mueller, and Rose Cobbett for constructive comments on the manuscript, Neil Martin, Robin Black, and Robert Burke from BMC Minerals and Dillon Hume from Equity Exploration for comments and conversations beneficial to this paper, and the BMC Minerals and Equity Exploration staff at the Kudz Ze Kayah exploration camp for their help during the 2018 and 2019 field seasons.

REFERENCES

Allen, R.L., Lundström, I., Ripa, M., Simeonov, A., and Christofferson, H., 1996a, Facies analysis of a 1.9 Ga, continental margin, back-arc, felsic caldera province with diverse Zn-Pb-Ag-(Cu-Au) sulfide and Fe oxide deposits, Bergslagen region, Sweden: Economic Geology, v. 91, p. 979–1006.

Allen, R.L., Weihed, P., and Svenson, S.A., 1996b, Setting of Zn-Cu-Au-Ag massive sulfide deposits in the evolution and facies architecture of a 1.9 ga marine volcanic arc, Skellefte district, Sweden: Economic Geology, v. 91, p. 1022–1053.

Allen, R.L., Weihed, P., Blundell, D., Crawford, T., Davidson, G., et al., 2002, Global comparisons of volcanic-associated massive sulphide districts: Geological Society of London, Special Publications, v. 204, p. 13–37.

Averyt, K.B., and Paytan, A., 2003, Empirical partition coefficients for Sr and Ca in marine barite: Implications for reconstructing seawater Sr and Ca concentrations: Geochemistry, Geophysics, Geosystems, v. 4, p. 1–14.

Barrett, T.J., and MacLean, W.H., 1994, Chemostratigraphy and hydrothermal alteration in exploration for VHMS deposits in greenstones and younger volcanic rocks: Geological Association of Canada, Short Course Notes, v. 11, p. 433–466.

Barrett, T.J., MacLean, W.H., and Tennant, S.C., 2001, Volcanic sequence and alteration at the Parys Mountain volcanic-hosted massive sulfide deposit, Wales, United Kingdom: Applications of immobile element lithogeochemistry: Economic Geology, v. 96, p. 1279–1305.

Barrote, V.R., McNaughton, N.J., Tessalina, S.G., Evans, N.J., Talavera, C., Zi, J.W., and McDonald, B.J., 2020, The 4D evolution of the Teutonic Bore

Camp VHMS deposits, Yilgarn Craton, Western Australia: Ore Geology Reviews, v. 120, article 103448.
Barth, M.G., McDonough, W.F., and Rudnick, R.L., 2000, Tracking the budget of Nb and Ta in the continental crust: Chemical Geology, v. 165, p. 197–213.
Bea, F., 1996, Controls on the trace element composition of crustal melts: Transactions of the Royal Society of Edinburgh-Earth Sciences, v. 87, p. 33–41.
Belford, S.M., Davidson, G.J., McPhie, J., and Large, R.R., 2015, Architecture of the Neoarchaean Jaguar VHMS deposit, Western Australia: Implications for prospectivity and the presence of depositional breaks: Precambrian Research, v. 260, p. 136–160.
Bischoff, J.L., and Rosenbauer, R.J., 1987, Phase separation in seafloor geothermal systems: American Journal of Science, v. 287, p. 953–973.
Boulton, A., 2002, GP4F polymetallic volcanic-hosted massive sulphide (VHMS) deposit, Finlayson Lake District, Yukon Territory: B.Sc. thesis (Honors), Victoria, Canada, University of Victoria, 47 p.
Bradshaw, G.D., Tucker, T.L., Peter, J.M., Paradis, S., and Rowins, S.M., 2001, Geology of the Wolverine polymetallic volcanic-hosted massive sulphide deposit, Finlayson Lake district, Yukon Territory, Canada, *in* Emond, D.S. and Weston, L.H. eds., Yukon exploration and geology 2000: Exploration and Geological Services Division, Yukon, Indian and Northern Affairs Canada, p. 269–287.
Bradshaw, G.D., Rowins, S.M., Peter, J.M., and Taylor, B.E., 2008, Genesis of the Wolverine volcanic sediment-hosted massive sulfide deposit, Finlayson Lake district, Yukon, Canada: Mineralogical, mineral chemical, fluid inclusion, and sulfur isotope evidence: Economic Geology, v. 103, p. 35–60.
Burnham, O.M., 2008, Trace element analysis of geological samples by inductively coupled plasma mass spectrometry (ICP-MS) at the Geoscience Laboratories: Revised capabilities due to method improvements: Summary of Field Work and Other Activities 2008: Ontario Geological Survey, Open File Report, v. 6226, p. 1–10.
Burnham, O.M., and Schweyer, J., 2004, Trace element analysis of geological samples by inductively coupled plasma mass spectrometry at the Geoscience Laboratories: Revised capabilities due to improvements to instrumentation: Summary of Field Work and Other Activities 2004: Ontario Geological Survey, Open File Report, v. 6145, p. 1–20.
Cas, R.A.F., and Wright, J.V., 1987, Volcanic successions: Modern and ancient: A geological approach to processes, products and successions: London, Allen & Unwin Ltd., 528 p.
Cathles, L.M., 2011, What processes at mid-ocean ridges tell us about volcanogenic massive sulfide deposits: Mineralium Deposita, v. 46, p. 639–657.
Cathles, L.M., Erendi, A.H.J., and Barrie, C.T., 1997, How long can a hydrothermal system be sustained by a single intrusive event?: Economic Geology, v. 92, p. 766–771.
Colpron, M., Nelson, J.L., and Murphy, D.C., 2006, A tectonostratigraphic framework for the pericratonic terranes of the Northern Canadian Cordillera: Geological Association of Canada, Special Paper 45, p. 1–23.
Converse, D.R., Holland, H.D., and Edmond, J.M., 1984, Flow rates in the axial hot springs of the East Pacific Rise (21°N): Implications for the heat budget and the formation of massive sulfide deposits: Earth and Planetary Science Letters, v. 69, p. 159–175.
DeWolfe, Y.M., Gibson, H.L., and Richardson, D., 2018, 3D reconstruction of volcanic and ore-forming environments of a giant VMS system: A case study from the Kidd Creek mine, Canada: Ore Geology Reviews, v. 101, p. 532–555.
Doyle, M.G., and Allen, R.L., 2003, Subsea-floor replacement in volcanic-hosted massive sulfide deposits: Ore Geology Reviews, v. 23, p. 183–222.
Doyle, M.G., and Huston, D.L., 1999, The subsea-floor replacement origin of the Ordovician Highway-Reward volcanic-associated massive sulfide deposit, Mount Windsor Subprovince, Australia: Economic Geology, v. 94, p. 825–844.
Fisher, R.V., 1966, Rocks composed of volcanic fragments and their classification: Earth Science Reviews, v. 1, p. 287–298.
Franklin, J.M., Lydon, J.W., and Sangster, D.F., 1981, Volcanic-associated massive sulfide deposits: Economic Geology, 75th Anniversary Volume, p. 485–627.
Franklin, J.M., Gibson, H.L., Jonasson, I.R., and Galley, A.G., 2005, Volcanogenic massive sulfide deposits: Economic Geology, 100th Anniversary Volume, p. 523–560.
Friesen, V.C., DeWolfe, Y.M., and Gibson, H.L., 2020, Volcanic reconstruction and geochemistry of the Powderhouse formation in the Paleoproterozoic VMS-hosting Chisel sequence, Snow Lake, Manitoba, Canada: Canadian Journal of Earth Sciences, v. 21, p. 1–21.
Gabrielse, H., Murphy, D.C., and Mortensen, J.K., 2006, Cretaceous and Cenozoic dextral orogen-parallel displacements, magmatism, and paleogeography, north-central Canadian Cordillera: Geological Association of Canada, Special Paper no. 46, p. 255–276.
Galley, A.G., 2003, Composite synvolcanic intrusions associated with precambrian VMS-related hydrothermal systems: Mineralium Deposita, v. 38, p. 443–473.
Galley, A.G., Watkinson, D.H., Jonasson, I.R., and Riverin, G., 1995, The subsea-floor formation of volcanic-hosted massive sulfide: Evidence from the Ansil, Rouyn-Noranda, Canada: Economic Geology, v. 90, p. 2006–2017.
Gamble, J.A., Wright, I.C., Woodhead, J.D., and McCulloch, M.T., 1995, Arc and back-arc geochemistry in the southern Kermadec arc-Ngatoro Basin and offshore Taupo volcanic zone, SW Pacific: Geological Society, London, Special Publication no. 81, p. 193–212.
Gemmell, B.J., and Large, R.R., 1992, Stringer system and alteration zones underlying the Hellyer volcanic-hosted massive sulfide deposit, Tasmania, Australia: Economic Geology, v. 87, p. 620–649.
Gibson, H.L., Morton, R.L., and Hudak, G.J., 1999, Submarine volcanic processes, deposits, and environments favourable for the location of volcanic-associated massive sulfide deposits: Reviews in Economic Geology, v. 8, p. 15–51.
Goodfellow, W.D., and Turner, R.J.W., 1989, Sulfur isotope variability in sediment-hosted massive sulfide deposits determined using the ion microprobe SHRIMP: 1. An example from the Rammelsberg orebody - A discussion: Economic Geology, v. 84, p. 451–452.
Green, T.H., 1995, Significance of Nb/Ta as an indicator of geochemical processes in the crust-mantle system: Chemical Geology, v. 120, p. 347–359.
Green, T.H., and Pearson, N.J., 1987, An experimental study of Nb and Ta partitioning between Ti-rich minerals and silicate liquids at high pressure and temperature: Geochimica et Cosmochimica Acta, v. 51, p. 55–62.
Halbach, P., Pracejus, B., and Marten, A., 1993, Geology and mineralogy of massive sulfide ores from the central Okinawa Trough, Japan: Economic Geology, v. 88, p. 2210–2225.
Hannington, M.D., de Ronde, C.E.J., and Petersen, S., 2005, Sea-floor tectonics and submarine hydrothermal systems: Economic Geology, 100th Anniversary Volume, p. 111–141.
Harrison, T.M., and Watson, E.B., 1983, Kinetics of zircon dissolution and zirconium diffusion in granitic melts of variable water content: Contributions to Mineralogy and Petrology, v. 84, p. 66–72.
Hart, T.R., Gibson, H.L., and Lesher, C.M., 2004, Trace element geochemistry and petrogenesis of felsic volcanic rocks associated with volcanogenic massive Cu-Zn-Pb sulfide deposits: Economic Geology, v. 99, p. 1003–1013.
Haymon, R.M., 1983, Growth history of hydrothermal black smoker chimneys: Nature, v. 301, p. 695–698.
Head, J.W., and Wilson, L., 2003, Deep submarine pyroclastic eruptions: Theory and predicted landforms and deposits: Journal of Volcanology and Geothermal Research, v. 121, p. 155–193.
Jamieson, J.W., Clague, D.A., and Hannington, M.D., 2014, Hydrothermal sulfide accumulation along the Endeavour Segment, Juan de Fuca Ridge: Earth and Planetary Science Letters, v. 395, p. 136–148.
Kerr, D.J., and Gibson, H.L., 1993, A comparison of the Horne volcanogenic massive sulfide deposit and intracauldron deposits of the Mine Sequence, Noranda, Quebec: Economic Geology, v. 88, p. 1419–1442.
Kranidiotis, P., and MacLean, W.H., 1987, Immobile elements as monitors of mass transfer in hydrothermal alteration: Phelps Dodge massive sulfide deposit, Matagami, Quebec: Economic Geology, v. 82, p. 951–962.
Lafrance, B., Gibson, H.L., and Stewart, M.S., 2020, Internal and external deformation and modification of volcanogenic massive sulfide deposits hydrothermal escape precipitation site discharge heat source: Reviews in Economic Geology, v. 21, p. 147–171.
Large, R.R., Allen, R.L., Blake, M.D., and Herrmann, W., 2001a, Hydrothermal alteration and volatile element halos for the Rosebery K Lens volcanic-hosted massive sulfide deposit, western Tasmania: Economic Geology, v. 96, p. 1055–1072.
Large, R.R., Gemmell, B.J., Paulick, H., and Huston, D.L., 2001b, The alternation box plot: A simple approach to understanding the relationship between alteration mineralogy and lithogeochemistry associated with volcanic-hosted massive sulfide deposits: Economic Geology, v. 96, p. 957–971.
Layton-Matthews, D., Peter, J.M., Scott, S.D., and Leybourne, M.I., 2008, Distribution, mineralogy, and geochemistry of selenium in felsic

volcanic-hosted massive sulfide deposits of the Finlayson Lake district, Yukon Territory, Canada: Economic Geology, v. 103, p. 61–88.

Layton-Matthews, D., Leybourne, M.I., Peter, J.M., Scott, S.D., Cousens, B., and Eglington, B.M., 2013, Multiple sources of selenium in ancient seafloor hydrothermal systems: Compositional and Se, S, and Pb isotopic evidence from volcanic-hosted and volcanic-sediment-hosted massive sulfide deposits of the Finlayson Lake district, Yukon, Canada: Geochimica et Cosmochimica Acta, v. 117, p. 313–331.

Le Maitre, R.W., Bateman, P., Dudek, A., Keller, J., Lameyre, J., Le Bas, M.J., Sabine, P.A., Schmid, R., Sorensen, H., and Streckeisen, A., 1989, Igneous rocks: A classification of igneous rocks and glossary of terms: London, Blackwell Scientific Publications, 256 p.

Lentz, D.R., 1998, Petrogenetic evolution of felsic volcanic sequences associated with Phanerozoic volcanic-hosted massive sulphide systems: The role of extensional geodynamics: Ore Geology Reviews, v. 12, p. 289–327.

Lesher, C.M., Goodwin, A.M., Campbell, I.H., and Gorton, M.P., 1986, Trace-element geochemistry of ore-associated and barren, felsic metavolcanic rocks in the Superior Province, Canada: Canadian Journal of Earth Sciences, v. 23, p. 222–237.

Lydon, J.W., 1984, Volcanogenic massive sulphide deposits Part 1: A descriptive model: Geoscience Canada, v. 11, p. 195–202.

——1988, Volcanogenic massive sulphide deposits Part 2: Genetic models: Geoscience Canada Reprint Series, v. 3, p. 1–29.

MacLean, W.H., 1988, Rare earth element mobility at constant inter-REE ratios in the alteration zone at the Phelps Dodge massive sulphide deposit, Matagami, Quebec: Mineralium Deposita, v. 23, p. 231–238.

MacLean, W.H., and Barrett, T.J., 1993, Lithogeochemical techniques using immobile elements: Journal of Geochemical Exploration, v. 48, p. 109–133.

Manor, M.J., and Piercey, S.J., 2018, Re-evaluating the chronostratigraphic framework for felsic volcanic and intrusive rocks of the Finlayson Lake region, Yukon-Tanana terrane, Yukon, *in* MacFarlane, K.E., ed., Yukon exploration and geology 2017: Yukon Geological Survey, p. 111–127.

——2019, Geochemistry of Devono-Mississippian volcanic and intrusive rocks of the Finlayson Lake district, Yukon-Tanana terrane, Yukon, *in* MacFarlane, K.E., ed., Yukon exploration and geology 2018: Yukon Geological Survey, p. 91–110.

Manor, M.J., Piercey, S.J., Wall, C.J., and Denisová, N., in press, High-precision CA-ID-TIMS U-Pb zircon geochronology of felsic rocks in the Finlayson Lake VMS district, Yukon: Linking Paleozoic basin-scale accumulation rates to the occurrence of subseafloor replacement-style mineralization: Economic Geology.

McDonald, M., Piercey, S.J., Layne, G., Pigage, L., and Piercey, G., 2018, Mineral assemblages, textures and in situ sulphur isotope geochemistry of sulphide mineralization from the Cyprus-type Ice volcanogenic massive sulphide (VMS) deposit, Yukon, Canada: Minerals, v. 8, p. 25.

McDonough, W.F., and Sun, S.S., 1995, The composition of the Earth: Chemical Geology, v. 120, p. 223–253.

McLennan, S.M., Bock, B., Hemming, S.R., Hurowitz, J.A., Lev, S.M., and McDaniel, D.K., 2003, The roles of provenance and sedimentary processes in the geochemistry of sedimentary rocks: Geological Association of Canada, GeoText 4, p. 7–38.

McPhie, J., Doyle, M.G., and Allen, R.L., 1993, Volcanic textures: A guide to interpretation of textures in volcanic rocks: Hobart, Australia, University of Tasmania, 198 p.

Monecke, T., Petersen, S., and Hannington, M.D., 2014, Constraints on water depth of massive sulfide formation: Evidence from modern seafloor hydrothermal systems in arc-related settings: Economic Geology, v. 109, p. 2079–2101.

Morris, G.A., Larson, P.B., and Hooper, P.R., 2000, "Subduction style" magmatism in a non-subduction setting: The Colville igneous complex, NE Washington State, USA: Journal of Petrology, v. 41, p. 43–67.

Mortensen, J.K., 1992, Pre-mid-Mesozoic tectonic evolution of the Yukon-Tanana terrane, Yukon and Alaska: Tectonics, v. 11, p. 836–853.

Mortensen, J.K., and Jilson, G.A., 1985, Evolution of the Yukon-Tanana terrane: Evidence from southeastern Yukon Territory: Geology, v. 13, p. 806–810.

Mumin, A.H., Scott, S.D., Somarin, A.K., and Oran, K.S., 2007, Structural controls on massive sulfide deposition and hydrothermal alteration in the south Sturgeon Lake Caldera, northwestern Ontario: Exploration and Mining Geology, v. 16, p. 83–107.

Murphy, D.C., 1998, Stratigraphic framework for syngenetic mineral occurrences, Yukon-Tanana terrane south of Finlayson Lake: A Progress Report, *in* Roots, C.F., ed., Yukon Exploration and Geology 1997: Exploration and Geological Services Division, Yukon, Indian and Northern Affairs Canada, p. 51–58.

Murphy, D.C., and Piercey, S.J., 1999, Finlayson project: Geological evolution of Yukon-Tanana terrane and its relationship to Campbell Range Belt, northern Wolverine Lake map area, southeastern Yukon, *in* Roots, C.F., and Emond, D.S., eds., Yukon exploration and geology 1998: Exploration and Geological Services Division, Yukon, Indian and Northern Affairs Canada, p. 47–62.

Murphy, D.C., Mortensen, J.K., Piercey, S.J., Orchard, M.J., and Gehrels, G.E., 2006, Mid-Paleozoic to early Mesozoic tectonostratigraphic evolution of Yukon-Tanana and Slide Mountain terranes and affiliated overlap assemblages, Finlayson Lake massive sulphide district, southeastern Yukon: Geological Association of Canada, Special Paper no. 45, p. 75–106.

Nelson, J., 1997, The quiet counter-revolution: structural control of syngenetic deposits: Geoscience Canada, v. 24, p. 91–98.

Nelson, J.L., Piercey, S.J., Murphy, D.C., and Geological Survey, B.C., 2006, Paleozoic tectonic and metallogenetic evolution of pericratonic terranes in Yukon, northern British Columbia and eastern Alaska: Geological Association of Canada, Special Paper no. 45, p. 323–360.

van Olden, K., Green, A., and Davidson, G., 2020, NI 43-101 feasibility study technical report Kudz Ze Kayah property, Yukon, Canada CSA Global Report n. R375.2020: CSA Global, 376 p., https://kudzzekayah.com/november-30-2020-ni-43-101-feasibility-study-technical-report-kudz-ze-kayah-property-yukon-canada/.

Parson, L.M., and Wright, I.C., 1996, The Lau-Havre-Taupo back-arc basin: A southward-propagating, multi-stage evolution from rifting to spreading: Tectonophysics, v. 263, p. 1–22.

Pearce, J.A., 1996, A user's guide to basalt discrimination diagrams: Geological Association of Canada, Short Course Notes, v. 12, p. 79–113.

——2008, Geochemical fingerprinting of oceanic basalts with applications to ophiolite classification and the search for Archean oceanic crust: Lithos, v. 100, p. 14–48.

Pearce, J.A., and Cann, J.R., 1973, Tectonic setting of basic volcanic rocks determined using trace element analyses: Earth and Planetary Science Letters, v. 19, p. 290–300.

Pearce, J.A., Harris, N.B.W., and Tindle, A.G., 1984, Trace element discrimination diagrams for the tectonic interpretation of granitic rocks: Journal of Petrology, v. 25, p. 956–983.

Peter, J.M., Layton-Matthews, D., Piercey, S.J., Bradshaw, G.D., Paradis, S., and Bolton, A., 2007, Volcanogenic-hosted massive sulphide deposits of the Finlayson Lake district, Yukon: Geological Association of Canada, Mineral Deposits Division, Special Publication no. 5, p. 471–508.

Piercey, S.J., 2001, Petrology and tectonic setting of mafic and felsic volcanic and intrusive rocks from the Finlayson Lake volcanic-hosted massive sulphide (VHMS) district: A record of mid-Paleozoic arc and back-arc magmatism and metallogeny: Ph.D. Thesis, Vancouver, Canada, University of British Columbia, 305 p.

——2011, The setting, style, and role of magmatism in the formation of volcanogenic massive sulfide deposits: Mineralium Deposita, v. 46, p. 449–471.

——2015, A semipermeable interface model for the genesis of subseafloor replacement-type volcanogenic massive sulphide (VMS) deposits: Economic Geology, v. 110, p. 1655–1660.

Piercey, S.J., and Colpron, M., 2009, Composition and provenance of the Snowcap assemblage, basement to the Yukon-Tanana terrane, Northern Cordillera: Implications for Cordilleran crustal growth: Geosphere, v. 5, p. 439–464.

Piercey, S.J., and Kamber, B.S., 2019, Lead isotope geochemistry of shales from the Wolverine volcanogenic massive sulfide deposit, Yukon: Implications for Pb isotope vectoring in exhalative ore systems: Economic Geology, v. 114, p. 47–66.

Piercey, S.J., Paradis, S., Murphy, D.C., and Mortensen, J.K., 2001, Geochemistry and paleotectonic setting of felsic volcanic rocks in the Finlayson Lake volcanic-hosted massive sulfide district, Yukon, Canada: Economic Geology, v. 96, p. 1877–1905.

Piercey, S.J., Murphy, D.C., Mortensen, J.K., and Paradis, S., 2002a, Boninitic magmatism in a continental margin setting, Yukon-Tanana terrane, southeastern Yukon, Canada: Geology, v. 29, p. 731–734.

Piercey, S.J., Mortensen, J.K., Murphy, D.C., Paradis, S., and Creaser, R.A., 2002b, Geochemistry and tectonic significance of alkalic mafic magmatism in the Yukon-Tanana terrane, Finlayson Lake region, Yukon: Canadian Journal of Earth Sciences, v. 39, p. 1729–1744.

Piercey, S.J., Mortensen, J.K., and Creaser, R.A., 2003, Neodymium isotope geochemistry of felsic volcanic and intrusive rocks from the Yukon-Tanana

terrane in the Finlayson Lake region, Yukon, Canada: Canadian Journal of Earth Sciences, v. 40, p. 77–97.
Piercey, S.J., Nelson, J.L., Colpron, M., Dusel-Bacon, C., Simard, R.-L.L., and Roots, C.F., 2006, Paleozoic magmatism and crustal recycling along the ancient Pacific margin of North America, Northern Cordillera: Geological Association of Canada, Special Paper no. 45, p. 281–322.
Piercey, S.J., Peter, J.M., Mortensen, J.K., Paradis, S., Murphy, D.C., and Tucker, T.L., 2008, Petrology and U-Pb geochronology of footwall porphyritic rhyolites from the Wolverine volcanogenic massive sulfide deposit, Yukon, Canada: Implications for the genesis of massive sulfide deposits in continental margin environments: Economic Geology, v. 103, p. 5–33.
Piercey, S.J., Squires, G.C., and Brace, T.D., 2014, Lithostratigraphic, hydrothermal, and tectonic setting of the Boundary volcanogenic massive sulfide deposit, Newfoundland Appalachians, Canada: Formation by subseafloor replacement in a Cambrian rifted arc: Economic Geology, v. 109, p. 661–687.
Piercey, S.J., Peter, J.M., and Herrington, R.J., 2015, Zn-rich volcanogenic massive sulphide (VMS) deposits, *in* Current Perspectives on Zinc Deposits: Irish Association for Economic Geology, p. 37–57.
Piercey, S.J., Gibson, H.L., Tardif, N., and Kamber, B.S., 2016, Ambient redox and hydrothermal environment of the Wolverine volcanogenic massive sulfide deposit, Yukon: Insights from lithofacies and lithogeochemistry of Mississippian host shales: Economic Geology, v. 111, p. 1439–1463.
Piercey, S.J., Beranek, L.P., and Hanchar, J.M., 2017, Mapping magma prospectivity for Cordilleran volcanogenic massive sulphide (VMS) deposits using Nd-Hf isotopes: Preliminary results, *in* MacFarlane, K.E., and Weston, L.H., eds., Yukon exploration and geology 2016: Yukon Geological Survey, p. 197–205.
Reimann, C., Filzmoser, P., and Garrett, R.G., 2005, Background and threshold: Critical comparison of methods of determination: Science of the Total Environment, v. 346, p. 1–16.
Rissmann, C., Nicol, A., Cole, J., Kennedy, B., Fairley, J., Christenson, B., Leybourne, M., Milicich, S., Ring, U., and Gravley, D., 2011, Fluid flow associated with silicic lava domes and faults, Ohaaki hydrothermal field, New Zealand: Journal of Volcanology and Geothermal Research, v. 204, p. 12–26.
Ross, P.-S., and Bédard, J.H., 2009, Magmatic affinity of modern and ancient subalkaline volcanic rocks determined from trace element discriminant: Canadian Journal of Earth Sciences, v. 46, p. 823–839.
Ruks, T.W., Piercey, S.J., Road, L., Pe, O., Ryan, J.J., Villeneuve, M.E., and Creaser, R.A., 2006, Mid- to late Paleozoic K-feldspar augen granitoids of the Yukon-Tanana terrane, Yukon, Canada: Implications for crustal growth and tectonic evolution of the Northern Cordillera: Bulletin of the Geological Society of America, v. 118, p. 1212–1231.
Sdrolias, M., and Müller, R.D., 2006, Controls on back-arc basin formation: Geochemistry, Geophysics, Geosystems, v. 7, p. 1–40.
Sebert, C., Hunt, J.A., and Foreman, I.J., 2004, Geology and lithogeochemistry of the Fyre Lake copper-cobalt-gold sulphide-magnetite deposit, southeastern Yukon: Open File 17, p. 46.
Shervais, J.W., 1982, Ti-V plots and the petrogenesis of modern and ophiolitic lavas: Earth and Planetary Science Letters, v. 59, p. 101–118.
Sibson, R.H., 2000, Fluid involvement in normal faulting: Journal of Geodynamics, v. 29, p. 469–499.
Sibuet, J.-C., Deffontaines, B., Hsu, S.-K., Thareau, N., Le Formal, J.-P., and Liu, C.-S., 1998, Okinawa Trough backarc basin: Early tectonic and magmatic evolution: Journal of Geophysical Research: Solid Earth, v. 103, p. 30,245–30,267.
De Silva, S.L., Riggs, N.R., and Barth, A.P., 2015, Quickening the pulse: Fractal tempos in continental arc magmatism: Elements, v. 11, p. 113–118.
Soltani Dehnavi, A., McFarlane, C., Lentz, D.R., McClenaghan, S., and Walker, J., 2019, Chlorite-white mica pairs' composition as a micro-chemical guide to fingerprint massive sulfide deposits of the Bathurst mining camp, Canada: Minerals, v. 9, p. 1–31.
Spitz, G., and Darling, R., 1977, Major and minor element lithogeochemical anomalies surrounding the Louvem copper deposit, Val d'Or, Quebec: Canadian Journal of Earth Sciences, v. 15, p. 1161–1169.
Thurston, P.C., Ayer, J.A., Goutier, J., and Hamilton, M.A., 2008, Depositional gaps in Abitibi greenstone belt stratigraphy: A key to exploration for syngenetic mineralization: Economic Geology, v. 103, p. 1097–1134.
Tornos, F., 2006, Environment of formation and styles of volcanogenic massive sulfides: The Iberian Pyrite Belt: Ore Geology Reviews, v. 28, p. 259–307.
Tornos, F., Peter, J.M., Allen, R.L., and Conde, C., 2015, Controls on the siting and style of volcanogenic massive sulphide deposits: Ore Geology Reviews, v. 68, p. 142–163.
Uyeda, S., and Kanamori, H., 1979, Back-arc opening and the mode of subduction: Journal of Geophysical Research, v. 84, p. 1049–1061.
Von Damm, K.L., 1990, Seafloor hydrothermal activity: Black smoker chemistry and chimneys: Annual Review of Earth and Planetary Sciences, v. 18, p. 173–204.
Watson, E.B., and Harrison, T.M., 1983, Zircon saturation revisited: Temperature and composition effects in a variety of crustal magma types: Earth and Planetary Science Letters, v. 64, p. 295–304.
Wedepohl, K.H., 1995, The composition of the continental crust: Geochemica et Cosmochimica Acta, v. 59, p. 1217–1232.
Whalen, J.B., Currie, K.L., and Chappell, B.W., 1987, A-type granites: Geochemical characteristics, discrimination and petrogenesis: Contributions to Mineralogy and Petrology, v. 95, p. 407–419.
White, J.D.L., 2000, Subaqueous eruption-fed density currents and their deposits: Precambrian Research, v. 101, p. 87–109.
White, J.D.L., and Houghton, B.F., 2006, Primary volcaniclastic rocks: Geology, v. 34, p. 677–680.
Winter, L.S., Tosdal, R.M., Franklin, J.M., and Tegart, P., 2004, A reconstructed Cretaceous depositional setting for giant volcanogenic massive sulfide deposits at Tambogrande, northwestern Peru: Society of Economic Geologists, Special Publication 11, p. 319–340.
Wright, I.C., Parson, L.M., and Gamble, J.A., 1996, Evolution and interaction of migrating cross-arc volcanism and backarc rifting: An example from the southern Havre Trough (35°20′-37°S): Journal of Geophysical Research: Solid Earth, v. 101, p. 22,071–22,086.
Zaw, K., and Large, R.R., 1992, The precious metal-rich South Hercules mineralization, western Tasmania: A possible subsea-floor replacement volcanic-hosted massive sulfide deposit: Economic Geology, v. 87, p. 931–952.

Nikola Denisová is currently a Ph.D. candidate at Memorial University of Newfoundland. Her project focuses on the genesis of the ABM replacement-style VMS deposit, Yukon, Canada. Nikola received her B.Sc. in Geology from Charles University in Prague and her M.Sc. in Geosciences at Luleå University of Technology. Prior to starting on her Ph.D. program in Canada, Nikola worked in iron, nickel, and gold exploration and mining projects in northern Sweden for four-and-a-half years.